

# Lattice dynamics in strongly correlated *d*- and *f*-electron metals

Przemysław Piekarz

Habilitation thesis



The H. Niewodniczański  
Institute of Nuclear Physics  
Polish Academy of Sciences

Kraków, December 2009

## Abstract

In the following dissertation, we study the dynamical properties of selected materials belonging to three groups of strongly correlated systems: the transition-metal spinel, magnetite ( $\text{Fe}_3\text{O}_4$ ), two actinide compounds  $\text{PuCoGa}_5$  and  $\text{UCoGa}_5$ , and the rare-earth metal Eu.

The Verwey transition in magnetite was investigated using the group theory and density functional theory calculations. We found that the structural transition from the high-temperature cubic to the low-temperature monoclinic phase is induced by two primary order parameters with symmetries  $X_3$  and  $\Delta_5$ . The electronic and crystal structures of both phases were calculated including the local Coulomb interaction  $U$  and Hund's exchange  $J$  between the  $3d$  electrons on Fe. For the cubic symmetry, the phonon dispersion curves were obtained using the direct method, and a significant dependence of the phonon spectrum on  $U$  was found. The electron-phonon coupling is strongly affected by electron correlations, leading in the case of the  $X_3$  mode to the metal-insulator transition. In the insulating state, the phonon order parameters stabilize the charge-orbital ordering on the octahedral Fe sites.

The electronic, structural, and phonon properties of the  $\text{PuCoGa}_5$  superconductor were studied using the first-principles methods. For the optimized electronic and crystal structure, the phonon dispersion curves and phonon density of states were calculated. It was found that phonon energies depend significantly on the on-site Hubbard interaction  $U$  between the  $5f$  electrons on Pu. Some transverse optical modes strongly soften up to 30% for  $U = 3$  eV. To verify this result, the dispersion curves were measured by the inelastic x-ray scattering at the synchrotron radiation source. A very good agreement between the theory and experiment indicates the importance of electron correlations in the lattice dynamics of  $\text{PuCoGa}_5$ . Using the calculated phonon density of states, the critical temperature was estimated, and the phonon mechanism of superconductivity was discussed. The phonon dispersion curves for the isostructural compound  $\text{UCoGa}_5$  were calculated for  $U = 0$ . A good agreement with the neutron experiment indicates the itinerant character of the  $5f$  electrons in this material.

The lattice dynamics of the rare-earth metal Eu was studied in the cubic  $bcc$  phase. All calculated phonon dispersions are stable at ambient conditions. The derived phonon density of states as well as the thermodynamic and elastic quantities for europium shows a very good agreement with the experimental data obtained by the resonant nuclear scattering.

## Streszczenie

W przedstawionej rozprawie habilitacyjnej badamy własności dynamiczne wybranych materiałów należących do trzech grup układów silnie skorelowanych: magnetyt ( $\text{Fe}_3\text{O}_4$ ), dwa związki aktynowców,  $\text{PuCoGa}_5$  i  $\text{UCoGa}_5$ , oraz metal ziem rzadkich, Eu.

Przejście Verweya w magnetycie zostało zbadane przy pomocy teorii grup i obliczeń opartych na teorii funkcjonału gęstości. Pokazano, że przejście strukturalne z wysokotemperaturowej fazy kubicznej do niskotemperaturowej fazy jednoskośnej indukowane jest przez dwa pierwotne parametry porządku o symetriach  $X_3$  i  $\Delta_5$ . Struktury elektronowe i krystaliczne dla obydwu faz zostały wyznaczone przy uwzględnieniu lokalnego oddziaływania kulombowskiego  $U$  i wymiany Hunda  $J$  między elektronami  $3d$  na żelazie. Dla symetrii kubicznej, obliczono fononowe krzywe dyspersji metodą bezpośrednią i znaleziono dużą zależność energii fononów od oddziaływania  $U$ . Sprzężenie elektron-fonon jest silnie modyfikowane korelacjami elektronowymi i w przypadku modu  $X_3$  prowadzi do przejścia metal-izolator. W fazie izolatora, fononowe parametry porządku stabilizują uporządkowanie ładunkowo-orbitalne na atomach Fe w położeniach oktaedrycznych.

Własności elektronowe, strukturalne i fononowe nadprzewodnika  $\text{PuCoGa}_5$  zbadano metodami obliczeniowymi z pierwszych zasad. Dla zoptymalizowanej struktury, wyznaczono fononowe relacje dyspersji i gęstości stanów. Pokazano, że energie fononowe zależą silnie od oddziaływania Hubbarda  $U$  dla elektronów w stanach  $5f$ . Energia niektórych modów optycznych zmniejsza się nawet do 30 % dla  $U = 3$  eV. Aby zweryfikować ten wynik, zmierzono krzywe dyspersji metodą nieelastycznego rozpraszania promieni X. Bardzo dobra zgodność między teorią i eksperymentem wskazuje na duży wpływ korelacji elektronowych na dynamikę sieci  $\text{PuCoGa}_5$ . Na podstawie wyliczonej fononowej gęstości stanów, wyznaczono temperaturę krytyczną i zbadano fononowy mechanizm nadprzewodnictwa. Dla izostrukturalnego związku  $\text{UCoGa}_5$  wyliczono fononowe relacje dyspersji dla  $U = 0$ . Dobra zgodność z pomiarami neutronowymi wskazuje na zdelokalizowany charakter stanów  $5f$  w tym związku.

Zbadana została dynamika sieci europu w fazie *bcc*. Wszystkie wyliczone gałęzie fononowe są stabilne przy zerowym ciśnieniu. Wyznaczona gęstość stanów fononowych, jak również wielkości termodynamiczne i elastyczne dla europu, bardzo dobrze zgadzają się z danymi eksperymentalnymi otrzymanymi metodą rezonansowego rozpraszania nuklearnego.

## List of original articles

[M1] *Mechanism of the Verwey transition in magnetite*, P. Piekarz, K. Parlinski, and A. M. Oleś, Phys. Rev. Lett. **97**, 156402 (2006)

[M2] *Origin of the Verwey transition in magnetite: Group theory, electronic structure, and lattice dynamics study*, P. Piekarz, K. Parlinski, and A. M. Oleś, Phys. Rev. B **76**, 165124 (2007)

[M3] *Order parameters in the Verwey phase transition*, P. Piekarz, K. Parlinski, and A. M. Oleś, Journal of Physics: Conf. Ser. **92**, 012164 (2007)

[P1] *First-principles study of phonon modes in PuCoGa<sub>5</sub> superconductor*, P. Piekarz, K. Parlinski, P. T. Jochym, A. M. Oleś, J. P. Sanchez, and J. Rebizant, Phys. Rev. B **72**, 014521 (2005)

[P2] *Probing the Coulomb interaction of the unconventional superconductor PuCoGa<sub>5</sub> by phonon spectroscopy*, S. Raymond, P. Piekarz, J.P. Sanchez, J. Serrano, M. Krisch, B. Janousova, J. Rebizant, N. Metoki, K. Kaneko, P.T. Jochym, A. M. Oleś, and K. Parlinski, Phys. Rev. Lett. **96**, 237003 (2006)

[P3] *Influence of local Coulomb interactions on lattice dynamics in PuCoGa<sub>5</sub> superconductor*, P. Piekarz, A. M. Oleś, K. Parlinski, and P. T. Jochym, Physica B **378-380**, 1029 (2006)

[U1] *Phonons in UCoGa<sub>5</sub>*, N. Metoki, K. Kaneko, S. Raymond, J.-P. Sanchez, P. Piekarz, K. Parlinski, A. M. Oleś, S. Ikeda, T. D. Matsuda, Y. Haga, Y. Onuki, and G. H. Lander, Physica B **378-380**, 1003 (2006)

[E1] *Lattice dynamics of Eu from nuclear inelastic scattering and first-principles calculations*, S. Stankov, P. Piekarz, A. M. Oleś, K. Parlinski, and R. Ruffer, Phys. Rev. B **78**, 180301 (2008)

# Contents

<b>1</b>	<b>Introduction</b>	<b>6</b>
1.1	Single-electron versus correlated state . . . . .	6
1.2	Phonons in transition-metal oxides . . . . .	7
1.3	Lattice dynamics in <i>f</i> -electron metals . . . . .	8
<b>2</b>	<b>Methods</b>	<b>10</b>
<b>3</b>	<b>Verwey transition in magnetite</b>	<b>12</b>
3.1	Historical review . . . . .	12
3.2	Order parameters . . . . .	13
3.3	Electronic structure . . . . .	14
3.4	Lattice dynamics . . . . .	15
3.5	Mechanism of the Verwey transition . . . . .	17
<b>4</b>	<b>Phonons in the actinide compounds</b>	<b>21</b>
4.1	Unconventional superconductivity in PuCoGa <sub>5</sub> . . . . .	21
4.2	Electron correlations and phonons in PuCoGa <sub>5</sub> . . . . .	22
4.3	Electron-phonon interaction . . . . .	25
4.4	Phonons in UCoGa <sub>5</sub> . . . . .	26
<b>5</b>	<b>Lattice dynamics of Eu</b>	<b>28</b>
<b>6</b>	<b>General remarks and summary</b>	<b>30</b>

# 1 Introduction

Structural and dynamical properties of materials depend on their electronic structures. The interatomic forces, which determine the positions of atoms and their movement, result from the electrostatic interactions between electrons; including those localized in the atomic core and itinerant valence electrons. In metals, forces between atoms are significantly screened by the valence electrons, so their distribution including spin polarization, determine to a large extent crystal dynamics. In insulators, the ionic interactions depends mainly on the electron configurations of the localized states, so the atom-like features (orbital occupancy, charge localization) become active and play important role in the atomic behavior. In strongly correlated materials, like transition-metal oxides or  $f$ -electron systems, local electron interactions radically modify the electronic structure through *e.g.* a metal-insulator transition. Such changes influence also lattice dynamics leading to new effects not observed in usual metals. Since many materials properties, also having practical applications like superconductivity or ferroelectricity, are strongly connected with lattice dynamics, deeper understanding of electron-phonon interrelations is of significant importance. This is the main subject of the presented dissertation.

## 1.1 Single-electron versus correlated state

Historically, the first electronic structure calculations were based on the models of non-interacting electrons moving in atom-like potentials [1]. It was assumed that all electronic interactions are contained in the effective field, composed of the repulsive electronic part and the attractive field of the nucleus. Since the electronic part of the potential depends on the wave functions one is going to find, the solution of the Schrödinger equation requires the iterative self-consistent approach. With inclusion of the Pauli exclusion principle this approach leads to the Hartree-Fock equations with the non-local exchange energy [2]. The exchange interaction reduces the repulsion between electrons with the same spin direction. Because of complicated calculations, the Hartree-Fock method is rarely applied for solids and has been used mainly for small systems (atoms, molecules).

A significant progress was associated with the formulation of the density functional theory (DFT) by Hohenberg, Kohn, and Sham [3, 4]. The basic theorem states that the total energy of a given system, including the exchange and correlation interactions, is a functional of the electron density, which can be uniquely determined by minimizing the ground state energy. In practical applications, the electron density and effective potential are obtained from the single-particle wave functions calculated self-consistently from the Schrödinger-type equations called the Kohn-Sham (KS) equations. The exact form of the exchange-correlation potential is unknown and the approximate functional must be used. In the most common local density approximation (LDA), the exchange-correlation potential is calculated from the uniform electron gas. The nonlocal effects can be taken into account partially by including the gradient expansion of the electron density within the generalized gradient approximation (GGA) [5]. During last 40 years, many efficient methods were developed to solve the KS equations and the DFT became a very powerful and basic tool for studying the electronic and structural properties of various types of materials [6].

However, there are systems where the DFT fails to describe correctly the electronic structure. According to the standard band theories, numerous transition-metal insulators, such as NiO or MnO, should be metallic due to the partial occupation of the  $d$ -electron bands. Indeed, the DFT ground state of transition-metal oxides is either metallic (CoO) or insulating with a strongly underestimated energy gap (NiO) [7]. Peierls was first who noticed that the Coulomb repulsion between electrons may prevent them from moving thus being the origin of the insulating behavior

[8]. Mott studied the mechanism of phase transition between the metallic and insulating state driven by local electron correlations [9]. To distinct from a typical band insulator, such material is called the *Mott insulator*. The basic and most popular model, which includes the on-site Coulomb interaction ( $U$ ) between electrons localized on the same atom was introduced by Hubbard [10]. The change of electron occupation by moving it from one atom to another costs large energy (proportional to  $U$ ) that strongly prevents charge fluctuations. For electrons in the more localized  $d$  and  $f$  orbitals, this local interaction is much stronger than in the extended  $s$  and  $p$  states. In the LDA, the exchange-correlation energy is obtained from the uniform electron gas, therefore, its value for the  $d$ - and  $f$ -electron systems is usually largely underestimated.

The electron potential for the localized states can be improved by adding to the DFT functional the Hubbard- $U$  energy term. It can be done on the static mean-field level within the LDA+ $U$  method [11]. This approach does not change the single-electron character of the Hamiltonian and can be solved accurately using the self-consistent procedure. When applied to the transition-metal monoxides [11] or high- $T_c$  cuprates [12], the LDA+ $U$  improves significantly the electronic structure (band gaps, magnetic moments) comparing to the LDA. Also in materials with complex interactions including spin, orbital, and lattice degrees of freedom (like the  $3d$ -perovskites), this method gives qualitatively better results than the LDA [13, 14, 15].

In strongly correlated metals, LDA+ $U$  enables to include partially effects of electron localization. A good example is plutonium, where the large discrepancy between the experimental and calculated volume (35 %) can be corrected using the realistic Hubbard interaction  $U = 4$  eV [16]. However, the dynamical effects like the formation of local moments or the Kondo effect can not be captured using static mean-field methods. In more sophisticated approach, the dynamical mean-field theory (DMFT), the many-body corrections are included by solving the single-impurity Anderson model using e.g. the quantum Monte Carlo technique [17]. The obtained energy spectrum contains information on the electronic self-energy and lifetimes not accounted for by the DFT. From the computational point of view, the DMFT is a highly demanding method and has been used so far only to the limited number of the  $d$ - and  $f$ -electron systems.

## 1.2 Phonons in transition-metal oxides

In materials, where the standard DFT fails to describe properly the electronic state, also the calculated phonon spectra show large discrepancies with the experiment. If the ground state followed from the DFT is metallic (instead of insulating), or the energy gap is too low, electron fluctuations and charge screening are usually overestimated, resulting in incorrect phonon energies [18]. In transition-metal oxides, strong softening of phonons is observed in the LDA calculations. When electron fluctuations are reduced by the local Coulomb repulsion, the screening of interatomic forces is weakened and phonon energies increase. A systematic improvement of calculated phonons for MnO [18], NiO [19], and CoO [20] was achieved, after including the on-site Coulomb interaction between  $3d$  electrons.

A large influence of electron correlations on phonons was revealed in the doped transition-metal perovskites. Particularly spectacular are phonon anomalies in the high- $T_C$  cuprate superconductors  $\text{La}_{2-x}\text{Sr}_x\text{CuO}_4$  [21, 22] and  $\text{YBa}_2\text{Cu}_3\text{O}_{6+x}$  [23]. A strong softening of the high-energy Cu-O breathing modes, is associated with the modification of charge screening due to a metal-insulator transition as well as the electron-phonon coupling. In addition, the anomalous discontinuity of phonon dispersions are induced by the inhomogeneous electronic state in the form of e.g. the charge-spin stripes [22, 24]. A strong softening and splitting of the bond-stretching modes was observed also in the doped nickelates [25] and bismuthates [26] indicating the important role of phonons in the ordered charge-spin states. Many of these effects were studied within the Hubbard or  $t$ - $J$  model [27], extended by the phonon terms. The results obtained by the

numerical methods, like the exact diagonalization [28] or quantum Monte Carlo [29], as well as the analytical techniques [30] point out to the unconventional character of the electron-phonon coupling in the doped Mott insulators. Although, the role of phonons in the high- $T_C$  cuprates is still not clear many interesting mechanisms of superconductivity involving local electron-phonon coupling were proposed and developed [31].

The electron-lattice coupling acquires new features due to orbital degrees of freedom. The best example is the interplay of the  $3d$  orbitals with lattice in manganites, which plays the crucial role in the colossal magnetoresistance [32]. The orbital ordering with the connected structural phase transition is driven by the Jahn-Teller (JT) distortion, which splits the degenerate  $e_g$  states on the  $Mn^{3+}$  ions. The anomalous broadening of the Raman modes responsible for the JT effect in  $LaMnO_3$  is observed below and above the structural transition [33]. In the slightly doped  $La_{1-x}Sr_xMnO_3$ , a giant phonon softening caused by the formation of the orbital polaron was revealed [34]. Such an orbital-phonon coupling renders new features of both the quasiparticle as well as the vibrational spectra [35], and induces local lattice distortions [36]. The orbital degrees of freedom coupled to lattice play important role in many other transition-metal perovskites, like  $YTiO_3$  and  $LaTiO_3$  [37].

In transition-metal spinels, the coupling between phonons and electronic degrees of freedom is strongly by the crystal geometry. A special character of spinels, having a general formula  $AB_2O_4$ , is associated with the existence of two nonequivalent cation sites: the tetrahedral  $A$  and the octahedral  $B$  positions. The latter form the pyrochlore lattice, consisting of the corner-sharing tetrahedra and being the origin of geometrical frustration of magnetic interactions and high degeneracy of the electronic state [38]. At low-temperatures, such system remains in a disordered state (spin glass) or lifts its degeneracy through a structural phase transition. In spinels, various types of the ordered states and electron-phonon mechanisms of phase transitions were revealed. In  $ZnMn_2O_4$ , the symmetry reduction to the tetragonal space group  $I4_1/amd$  and the orbital ordering is driven by the JT effect [39]. The tetragonal distortion in  $ZnCr_2O_4$  induces the AF order with the spin gap similarly to the spin-Peierls systems [40]. The metal-insulator transition in  $MgTi_2O_4$  is induced by the spin-singlet formation and dimerization of the atomic bonds [41]. In some cases, the AF state, which breaks the cubic symmetry, influences significantly the phonon frequencies due to spacial modulation of the exchange coupling (spin-phonon interaction) [42]. Recently, a large splitting of the infrared modes in  $FeCr_2O_4$  induced by the magnetic ordering with no structural component has been detected [43].

The best known material crystallizing in the spinel structure is magnetite ( $Fe_3O_4$ ). The phase transition observed at  $T_V = 122$  K, known as the Verwey transition (VT), fascinated people since its discovery more than 70 years ago. Recent experimental and theoretical studies revealed a cooperative charge-orbital-phonon nature of the VT. Our studies, presented in [M1,M2,M3], established the order parameters of the VT and the electron-phonon mechanism leading to the charge-orbital ordering in the low-symmetry monoclinic phase. The main results of these studies are presented in Sec. 3.

### 1.3 Lattice dynamics in $f$ -electron metals

Lattice dynamics studies in the lanthanides and actinides are very limited due to the experimental difficulties such as radioactivity, high reactivity, small single crystals, and high neutron absorption. Theoretical problems with description of complex electronic and structural properties of actinides result from a dual itinerant-localized character of the  $5f$  electrons. In light actinides (Th-Np), the  $5f$  states are delocalized and take part in atomic bonding, while in heavy ones (Am and beyond), electrons are completely localized in cores [44]. Plutonium lies at the border between these two groups, and it is the most complex element in the periodic table.

A specific character of actinides is reflected by unusual properties of lattice dynamics. In Th, the phonon dispersions with two Kohn anomalies [45] were successfully calculated by Bouchet *et al.* [46], indicating the itinerant character of the  $5f$  electrons in this metal. Uranium has much complicated structure and some extraordinary features of the lattice dynamics have been revealed. Firstly, phonon anomalies related to the charge-density wave (CDW) formation at  $T = 43$  K were observed by the inelastic neutron scattering (INS) measurements [47, 48]. Additionally, a strong temperature dependence of phonon energies [49] and the formation of an intrinsic localized mode at high temperatures [50] were found. The calculations successfully reproduced phonon softening induced by the CDW and energies of the acoustic modes [51]. The optic modes, however, show large discrepancy with the experiment, indicating that not all electronic interactions were correctly included. In  $\delta$ -Pu, the phonon dispersion curves were first calculated using the DMFT method [52]. The qualitative predictions: the Kohn anomaly in the transverse acoustic (TA)[011] branch and strong softening of the TA[111] mode were then verified by the inelastic x-ray scattering (IXS) [53], however, some quantitative discrepancies are not well understood.

Many actinide compounds containing U or Pu display remarkable superconducting properties at low-temperatures. Most of them belong to the heavy-fermion systems, like UPt<sub>3</sub> or UBe<sub>13</sub>, with characteristic large effective electron masses ( $m^* \sim 200m_e$ ) [54]. In some of them, the superconducting state coexists with the ferromagnetism (UGe<sub>2</sub>, URhGe), indicating the unconventional (non-phononic) pairing mechanism promoted by magnetic interactions. In fact, the role of phonons in the  $f$ -electron superconductors is not well understood, and both the experimental and theoretical studies of lattice dynamics in those materials are very rare. The first *ab initio* studies of phonons in the actinide compounds were performed for the superconductor PuCoGa<sub>5</sub> [**P1,P2,P3**] and UCoGa<sub>5</sub> [**U1**], and they will be presented in Sec. 4.

The partially filled  $4f$  states in rare earths (RE) exhibit even more localized character than the  $5f$  states in actinides and the  $3d$  states in transition metals. It is the origin of high magnetic moments and very diverse electronic properties. Due to a localized character of the  $4f$  electrons the bonding properties of lanthanides are mainly determined by the valence *spd* electrons. Some effect of the  $4f$  electrons on interatomic forces and phonon frequencies may result from the hybridization between the  $4f$  and valence states [55]. This effect can be largely enhanced under high pressure, which induces the volume collapse and delocalization of the  $4f$  electrons (observed e.g. in Ce). To study such effects, the phonon spectrum should be investigated by the experimental as well as the first-principles methods. Accurate phonon calculations are therefore necessary to complete our knowledge about lanthanides, including also the mechanisms of phase transitions in these materials [56]. In a few cases, the dispersion curves were calculated using the Born-von Karman model and fitted to the INS measurements [57, 58, 59]. Our studies of europium presented in [**E1**] and discussed in Sec. 5, are the first *ab initio* calculations of phonon spectrum of the RE element.

## 2 Methods

The crystal and electronic structures of the considered materials were studied using the Vienna Ab Initio Simulation Package (VASP) [60]. This program is based on the DFT and it solves the KS equations using the selfconsistent iterative diagonalization procedure. All calculations are performed in the supercell with the periodic boundary conditions, which simulates the infinite crystal. The electron potential and wave functions are calculated in the entire volume, divided into the atomic core and interatomic (bonding) regions, using the Blöchl's projector augmented-wave (PAW) method [61]. It was implemented in the VASP program by Kresse and Joubert [62]. This method joins a high accuracy of the all-electron methods, like LAPW and LMTO, with an efficiency and simplicity of the pseudopotential approaches. Similarly to the latter methods, the PAW technique uses the pseudo wave functions  $\tilde{\Psi}(\mathbf{r})$ , expanded in the plane-wave basis, which exactly describe one-electron states in the bonding region. A smooth continuation of the pseudofunction  $\tilde{\Psi}(\mathbf{r})$  in the atomic core approximates the exact wave function  $\Psi(\mathbf{r})$ , which rapidly oscillates and changes its sign in this region. Therefore,  $\tilde{\Psi}(\mathbf{r})$  is much more convenient for the crystal structure optimization, which mainly depends on the electron density in the bonding region. Since, the PAW method provides the exact linear transformation between both the wave functions  $\Psi(\mathbf{r})$  and  $\tilde{\Psi}(\mathbf{r})$ , all electronic properties of the core can be recovered in the course of calculations.

As discussed in the previous section, the main approximation in the DFT concerns the exchange-correlation energy. We used the GGA functional derived by Perdew, Burke, and Ernzerhof (PBE) [63]. Gradient corrections beyond the LDA are particularly important for the  $f$ -electron elements [64]. There are a few more necessary approximations. The plane-wave expansion can be limited since the contribution from the high-energy states above some cut-off  $E_{cut}$  is negligible. This energy cut-off is usually determined "empirically" by checking the convergence of the ground state energy and other parameters with the increasing value of  $E_{cut}$ . Using the same procedure one can determine the number of  $\mathbf{k}$ -points needed for the integration in the reciprocal space. The optimal  $\mathbf{k}$ -point grid is generated by the Monkhorst-Pack scheme [65]. Usually, only the valence states are included in the electron basis. In the case of magnetite, we used eight electrons for Fe: $3d^64s^2$  and six ones for O: $2s^22p^4$ . For actinides and lanthanides, much more electrons were taken; Pu(16): $6s^26p^65f^67s^2$ , U(14): $6s^26p^66d^15f^37s^2$ , and Eu(17): $5s^25p^64f^76s^2$ .

The local Coulomb interactions between electrons in the  $d$  and  $f$  states are included within the LDA+ $U$  method [11]. VASP uses the rotationally invariant version introduced by Liechtenstein *et al.* [13]. In connection with the GGA this method is called GGA+ $U$ . The basic assumption is made that the total energy of the whole crystal can be written in the form

$$E_{tot} = E_{GGA} + E_U - E_{dc}, \quad (1)$$

where  $E_{GGA}$  is the energy functional within the GGA,  $E_U$  describes the on-site interactions, and  $E_{dc}$  is the double-counting correction equals to the average electron-electron interaction, already included in the GGA. The on-site interaction energy  $E_U$  is parametrized by the Coulomb repulsion  $U$  and the Hund's exchange energy  $J$ . These interactions are written in the form of the Hubbard-type model

$$E_U = U \sum_{i,\alpha,\beta,\sigma} n_{i\alpha\sigma} n_{i\beta\bar{\sigma}} + (U - J) \sum_{i,\alpha \neq \beta,\sigma} n_{i\alpha\sigma} n_{i\beta\sigma}, \quad (2)$$

where  $i$  runs over all atomic sites,  $\alpha$  and  $\beta$  denote the  $d$  or  $f$  orbitals, and  $\sigma = \uparrow, \downarrow$  is the spin component ( $\bar{\sigma} = -\sigma$ ). The spin- and orbital-dependent electron occupancies  $n_{i\alpha\sigma}$  are obtained by the projection of the PAW function  $\Psi_\sigma$  onto the spherical harmonics:  $n_{i\alpha\sigma} = |\langle i, \alpha | \Psi_\sigma \rangle|^2$ . The

first term in Eq. (1) describes the Coulomb repulsion between electrons with antiparallel spins. In the present approximation, the intraorbital and inter-orbital interactions are the same and equal  $U$ . In the accurate approach, the latter coupling is smaller,  $U' = U - 2J$ . In the second term, the inter-orbital interactions for electrons with parallel spins are reduced by the exchange coupling  $J$ . The double-counting term reads

$$E_{dc} = \frac{1}{2}Un(n-1) - \frac{1}{2}J[n_{\uparrow}(n_{\uparrow}-1) + n_{\downarrow}(n_{\downarrow}-1)], \quad (3)$$

where  $n = n_{\uparrow} + n_{\downarrow}$  is the average electron occupancy of all orbitals on one atomic site.

The effective one-electron potential is obtained by the functional derivative of the total energy  $E_{tot}$  over the charge density, taking into account the density of particular orbitals  $n_{\alpha\sigma}(\mathbf{r})$ . The derived potential depends not only on the electron density, but also on two parameters  $U$  and  $J$ . There are a few ways to determine their values. They can be expressed as functions the Slater integrals:  $U = F^0$  and  $J = \frac{1}{14}(F^2 + F^4)$  (for  $d$  electrons), which are given in terms of the Racah parameters  $A$ ,  $B$ , and  $C$  [66]. Usually, the atomic values of  $U$  are strongly overestimated comparing to realistic interactions in solids that are screened by the itinerant  $s$  or  $p$  electrons. The effect of screening can be taken into account using the constrained DFT method. The obtained in this way value of  $U$  for the Fe( $3d$ ) states in magnetite equals approximately 4 eV [67], and such value was taken in our calculations. The exchange parameter  $J = 0.8$  eV was obtained from the formula  $J = \frac{5}{2}C + B$  [68], using the Racah parameters for Fe<sup>2+</sup> ions:  $B = 0.131$  eV and  $C = 0.484$  eV. For plutonium, we used the Coulomb energy  $U = 3$  eV estimated from the spectroscopic measurements [69].

For given parameters  $U$  and  $J$ , the ground state of a crystal is found by the minimization of the total energy with respect to the electron density and all lattice parameters; lattice constants and atom positions. The force acting on the  $i$ th atom is determined by the Hellmann-Feynman (HF) theorem,  $F_i = -\frac{dE_{tot}}{du_i}$  [70], so, the condition  $E_{tot} = \min$  is equivalent to the equilibrium state with all forces equal to zero. In VASP, the optimization of a crystal is carried out using the conjugate gradient and quasi-Newton procedures [60], and it is continued until all residual forces and stress-tensor elements are less than the assumed values. The optimized crystal structure is a starting point for the lattice dynamics studies.

Phonon dispersion curves and phonon DOSs were calculated using the direct method developed by Parlinski *et al.* [71] and implemented in the PHONON program [72]. The method is based on calculations of the HF forces by displacing atoms, one at a time, from the equilibrium positions. Necessary displacements are uniquely determined by the crystal symmetry and the number of non-equivalent atoms in the supercell. The force acting on the  $\nu$ th atom is related to the atom displacements by the formula

$$F_{\alpha}(\nu) = -\sum_{\mu,\beta} \Phi_{\alpha\beta}(\nu,\mu)u_{\beta}(\mu), \quad (4)$$

where  $\alpha = x, y, z$  is the direction in a crystal. The force-constants matrix elements  $\Phi_{\alpha\beta}$  are determined from Eq. (4) using the singular value decomposition method. The dynamical matrix  $D_{\alpha\beta}(\mathbf{k})$  is constructed by the Fourier transformation of the force-constant matrix and then diagonalized for the set of  $\mathbf{k}$ -points in the reciprocal space,  $D(\mathbf{k})\mathbf{e}(\mathbf{k}) = E^2(\mathbf{k})\mathbf{e}(\mathbf{k})$ . This procedure provides the energy dispersion curves  $E_j(\mathbf{k})$  and polarization vectors  $\mathbf{e}_j(\mathbf{k})$ , where  $j = 1, \dots, 3N$  numerates the phonon branches, and  $N$  is the number of non-equivalent atoms in the primitive cell. Since, the HF forces and force constants are calculated from the total energy, Eq. (1), the resulting phonon energies and polarization vectors depend on the local interactions  $U$  and  $J$ .

### 3 Verwey transition in magnetite

*Understanding magnetite means  
understanding solid state physics*  
Shuichi Iida (1971)

#### 3.1 Historical review

Magnetite is the oldest known magnetic mineral naturally occurring on Earth. Discovered in ancient Greece, magnetite was used in compasses in Europe and China in the medieval times. A first indication of the phase transition at low temperatures was reported in the magnetic susceptibility measurements in 1913 [73]. Then it was detected as the anomalous peak in specific heat observed around  $T_V = 120$  K [74]. Measuring the electric resistivity as a function of temperature, Verwey observed a sharp change of its value at  $T_V$  [75]. Below  $T_V$  magnetite has about two orders of magnitude higher resistivity and shows typical insulating behavior. Above  $T_V$  the conductivity increases, and magnetite becomes a metal at higher temperatures.

In 1947, Verwey proposed the electronic mechanism of the phase transition associated with the charge ordering on the Fe ions [76]. At room temperature, magnetite crystallizes in the cubic face-centered structure with the space group symmetry  $Fd\bar{3}m$ . Fe ions occupy the tetrahedral  $A$  sites with four oxygen neighbors and the octahedral  $B$  sites surrounded by six oxygen atoms. In the ionic model, all  $A$  sites are occupied by the trivalent  $\text{Fe}^{3+}$  ions, while on the  $B$  sites there is a random distribution of equal numbers of  $\text{Fe}^{2+}$  and  $\text{Fe}^{3+}$  ions. Magnetic moments at the  $A$  and  $B$  sites are aligned antiparallely, giving the average magnetic moment  $4\mu_B$  per formula unit. In the metallic state, the electrical conductivity results from the exchange of electrons between  $\text{Fe}^{+2}$  and  $\text{Fe}^{+3}$  ions in the  $B$  sites. Verwey assumed that at lower temperatures electron fluctuations are frozen and below  $T_V$  a static charge order (CO) takes place at the iron  $B$  sites. In this model, Fe ions with different valency +2 and +3 occupy the alternative planes perpendicular to the  $c$  axis.

This simple ionic picture was questioned, when diffraction studies below  $T_V$  revealed changes in the crystal structure, not consistent with the Verwey model. In particular, the observation of half-integer reflections  $(h, k, l + \frac{1}{2})$  in neutron scattering indicated the doubling of the unit cell along the  $c$  axis [77]. The neutron diffuse scattering allows to identify the phonon at  $\mathbf{k}_\Delta = (4, 0, \frac{1}{2})$  with the  $\Delta_5$  symmetry, which induces critical fluctuations above  $T_V$  [78]. Lorenz and Ihle described the VT as a condensation of a coupled charge density-phonon  $\Delta_5$  mode, which breaks the crystal symmetry and induces electron localization below  $T_V$  [79]. Further neutron measurements revealed even stronger diffuse scattering with maxima at the  $\Gamma$  and  $X$  points [80]. Many other observations like the softening of the elastic constant  $c_{44}$  [81], oxygen isotope effect [82], strong dependence of  $T_V$  on stoichiometry [83] and impurity doping [84] indicated the important role of the lattice in the VT.

Although the Verwey model was not confirmed, many experiments were planned in order to prove or reject the existence of CO below  $T_V$ . The nuclear magnetic resonance studies [85, 86] revealed 16 nonequivalent  $\text{Fe}(B)$  sites below  $T_V$  in agreement with the monoclinic symmetry [87]. On the basis of very accurate diffraction neutron and x-ray studies, a simpler model of the low-temperature phase was introduced with four non-equivalent  $B$  sites [88]. Analyzing the Fe-O distances, the CO scheme was found with the fractional charge disproportionation at the  $\text{Fe}(B)$  sites. In this model,  $B_1$  and  $B_4$  have larger electron occupation and smaller valence +2.4, while two others  $B_2$  and  $B_3$  have lower electron density and the larger valence +2.6. In 2004, two independent theoretical LDA+ $U$  studies of the experimental monoclinic  $P2/c$  structure confirmed the existence of the fractional CO at the  $B$  sites [89, 90]. In addition,

these calculations revealed the orbital ordering of the occupied  $t_{2g}$  states at the  $B_1$  and  $B_4$  sites. Experimentally, the charge-orbital ordering has been studied using the resonant x-ray scattering, which exploits a strong energy dependence of Bragg peaks close to the absorption edge. Although, some contradiction results were published [91], many convincing results supporting the fractional charge and orbital ordering were presented during last few years [92, 93, 94, 95, 96].

In spite of this significant progress, the fundamental questions about the origin of the VT have remained open. It was not clear what is the main driving force of the transition: the Coulomb interaction or the lattice instability? What is the order parameter of the VT? What is the relation between the the electron-phonon interaction and the charge-orbital ordering observed below  $T_V$ ? In a series of papers [M1,M2,M3], we addressed these questions using the theoretical approach which combines the analytical group theory analysis with the computational *ab initio* techniques. The main results are presented in the following sections.

### 3.2 Order parameters

In the Landau theory of structural phase transitions, the order parameter (OP) is associated with a soft mode, which reduces the high-symmetry space group  $\mathcal{H}$  to one of its subgroups  $\mathcal{L} \subset \mathcal{H}$ . The soft mode is characterized by the irreducible representation (IR) of the high-symmetry group  $\mathcal{H}$ . The OP which determines the symmetry of the low-symmetry phase is called a *primary* OP. A *secondary* OP is associated with a phonon mode which reduces the symmetry of the space group  $\mathcal{H}$  to an intermediate space group  $\mathcal{I}$ , such that  $\mathcal{I}$  becomes a subgroup to  $\mathcal{H}$ , and a supergroup for  $\mathcal{L}$ , i.e.,  $\mathcal{L} \subset \mathcal{I} \subset \mathcal{H}$ . If the low-symmetry phase is generated by a simultaneous condensation of a few phonons, a phase transition can be describe by two or more OPs. Thus, in general  $N$  primary OPs reduce the high-symmetry space group  $\mathcal{H}$  into  $\mathcal{L}_1, \mathcal{L}_2, \dots, \mathcal{L}_N$  space groups, and the final low-symmetry space group  $\mathcal{L}$  is an intersection of all these subgroups. The secondary OPs are associated with phonons which reduce the symmetry of the high-symmetry space group to intermediate space groups  $\mathcal{I}_n$ , such that  $\mathcal{L}_n \subset \mathcal{I}_n \subset \mathcal{H}$ , where  $n = 1, 2, \dots N$ .

We performed the group theory analysis of the symmetry reduction from the high-symmetry space group  $\mathcal{H} = Fd\bar{3}m$  to the low-symmetry monoclinic phase  $\mathcal{L} = P2/c$ . The details of the analysis were presented in [M1,M2]. To obtain the list of possible intermediate  $\{\mathcal{I}_n\}$  and low-symmetry  $\{\mathcal{L}_n\}$  space groups, we used two computer codes: COPL [97] and ISOTROPY [98]. We found that there is no single IR which reduces  $Fd\bar{3}m$  to low-symmetry  $\mathcal{L} = P2/c$ . This means that the phase transition in  $\text{Fe}_3\text{O}_4$  is driven by *at least* two primary OPs. A closer inspection of space group-subgroup relationships, leads us to the conclusion that in principle there are five primary OPs:  $X_3, \Delta_2, \Delta_4, \Delta_5, T_{2g}$ , and five secondary ones:  $A_{1g}, E_g, T_{1g}, X_1, T_{2g}$  (see Tab. I in [M1]). Depending on the number of non-zero components the IR  $T_{2g}$  can be classified as the primary or the secondary OP.

The  $X_3$  mode is the only primary OP at the zone boundary and its appearance is crucial to generate the monoclinic symmetry (see Tab. III in [M2]). Experimentally, the atomic displacements with the  $X_3$  symmetry were found in the neutron diffuse scattering detected above  $T_V$  [100]. At the  $\mathbf{k}_\Delta$  point, there are three possible OPs and the intersection of either of these modes with  $X_3$  induces the  $P2/c$  symmetry. The experiments revealed that the dominant component of atomic displacements at  $\mathbf{k}_\Delta$ , observed in the diffuse scattering [78] as well as in the diffraction studies [87], has the  $\Delta_5$  symmetry. The contribution of the  $T_{2g}$  OP, which couples to the shear strain, was suggested by the observed softening of the  $c_{44}$  elastic constant [99]. The  $T_{2g}$  phonon reduces the cubic symmetry ( $Fd\bar{3}m \rightarrow Imma$ ), but it does not change the final monoclinic  $P2/c$  space group.

The main result of the group theory analysis implies that the monoclinic symmetry is induced

by two primary OPs  $X_3$  and  $\Delta_5$ , and the reduction diagrams can be written

$$\begin{aligned} Fd\bar{3}m &\rightarrow [X_3, \mathbf{k} = (0, 0, 1)] \rightarrow Pmna(2), \\ Fd\bar{3}m &\rightarrow \left[ \Delta_5, \mathbf{k} = \left( 0, 0, \frac{1}{2} \right) \right] \rightarrow Pbcm(4), \end{aligned} \quad (5)$$

where the increase of the primitive cell is indicated in brackets. The intersection of these two groups gives the  $P2/c$  space group

$$Pmna \cap Pbcm = P2/c. \quad (6)$$

The secondary OPs do not reduce further the crystal symmetry but they become active at the VT by coupling to the primary OPs or to the external fields. This coupling is described by the Landau free energy expanded in a series of non-zero components of the OPs, and the order of coupling terms is determined by the group theory. In [M3], we performed the analysis of the VT within the Landau theory including two primary OPs:  $X_3(g)$  and  $\Delta_5(q)$ , one secondary OP:  $T_{2g}(\eta)$ , and the shear-strain ( $\epsilon$ ). The free energy can be written in the form

$$\mathcal{F} = \mathcal{F}_0 + \frac{\alpha_1}{2}g^2 + \frac{\beta_1}{4}g^4 + \frac{\gamma_1}{6}g^6 + \frac{\alpha_2}{2}q^2 + \frac{\beta_2}{4}q^4 + \frac{\delta_1}{2}g^2q^2 + \frac{\alpha_3}{2}\eta^2 + \frac{\alpha_4}{2}\epsilon^2 + \frac{\delta_2}{2}\eta g^2 + \frac{\delta_3}{2}\epsilon g^2 + \delta_4\eta\epsilon, \quad (7)$$

where  $\mathcal{F}_0$  is a constant part of the potential. We assume that  $\beta_1 > 0$ ,  $\beta_2 > 0$  and  $\gamma_1 > 0$  to ensure the stability of the potential at high temperatures. For the second-order terms we assume standard temperature behavior  $\alpha_i = a_i(T - T_{ci})$  near the critical temperature  $T_{ci}$  for  $i = 1, 2, 3$ . The coefficient  $\alpha_4$  is the shear elastic constant at high temperatures ( $C_{44}^0$ ). Taking first derivatives of  $\mathcal{F}$  over the OPs we obtain the dependence between  $g$  and  $q$

$$q^2 = -\frac{\delta_1 g^2 + \alpha_2}{\beta_2}, \quad (8)$$

which has three possible solutions: (i)  $g = 0$  and  $q^2 = -\frac{\alpha_2}{\beta_2}$  if  $\alpha_2 < 0$  ( $Pbcm$ ), (ii)  $q = 0$  and  $g^2 = -\frac{\alpha_2}{\delta_1}$  if  $\alpha_2 > 0$  and  $\delta_1 > 0$  or  $\alpha_2 < 0$  and  $\delta_1 > 0$  ( $Pmna$ ), (iii)  $g \neq 0$  and  $q \neq 0$  ( $P2/c$ ). In the brackets we put the space group symbols, which characterize the low-symmetry phases. The solution (iii) which corresponds to the experimentally observed monoclinic phase requires simultaneous condensation of both primary OPs. The necessary condition for this is a negative value of  $\delta_1$ . For  $\delta_1 < 0$ , Eq. (8) has a non-zero solution provided that  $|\delta_1|g^2 > \alpha_2$ . It implies that for  $\alpha_2 > 0$  ( $T > T_{c2}$ ), the phase transition occurs when  $g$  exceeds a critical value  $\frac{\alpha_2}{|\delta_1|}$ , so it has a discontinuous (first-order) character. In [M3], we derived also the temperature dependence of the elastic constant  $c_{44}$ , which shows a critical softening above  $T_V$ , and found a good agreement with the experiment and previous calculations [99].

### 3.3 Electronic structure

The electronic structure of the high-temperature cubic phase of magnetite can be understood starting from the electron configurations of  $\text{Fe}^{2+}$  and  $\text{Fe}^{3+}$  ions. Due to the Hund's exchange both ionic configurations correspond to the high-spin states  $\text{Fe}^{2+}$ :  $t_{2g\uparrow}^3 t_{2g\downarrow} e_{g\uparrow}^2$  ( $S=2$ ) and  $\text{Fe}^{3+}$ :  $t_{2g\uparrow}^3 e_{g\uparrow}^2$  ( $S=5/2$ ). The exchange coupling causes the splitting of the majority up-spin and minority down-spin states and shifts one type of the states with respect to the other. Consequently only the down-spin states occupy the energy levels at the Fermi energy ( $E_F$ ). Additionally, the  $3d$  states are split into  $t_{2g}$  and  $e_g$  orbitals by the crystal field, which is much larger at the  $\text{Fe}(B)$  atoms than at the  $\text{Fe}(A)$  ones. All these features are visible in Fig. 1, where the electron

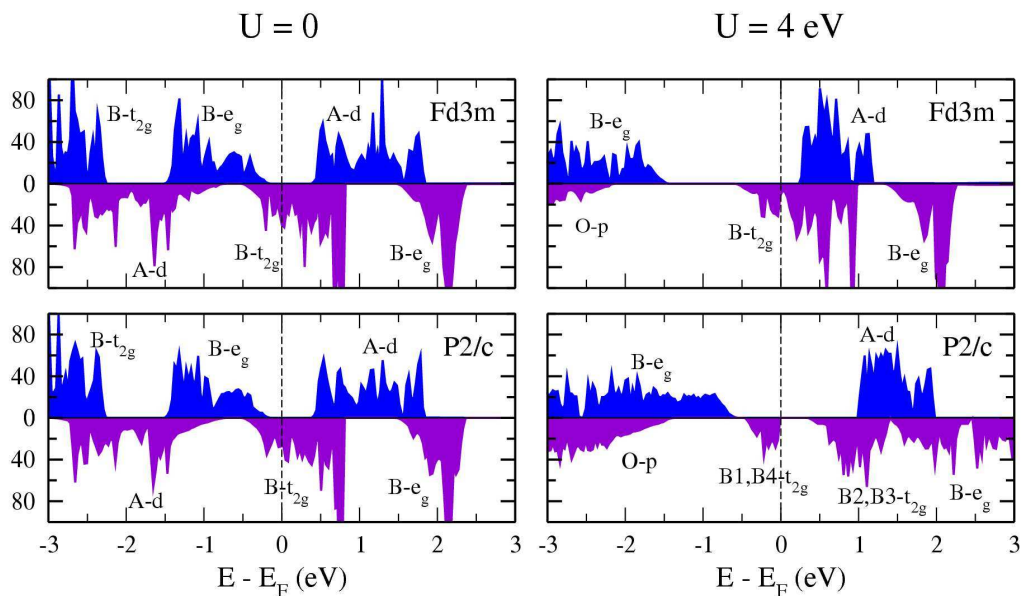


Figure 1: Electronic DOSs of  $\text{Fe}_3\text{O}_4$  for the cubic (top) and monoclinic (bottom) phase with  $U = 0$  (left) and  $U = 3$  eV (right).

density of states (DOS) for up-spins and down-spins obtained at  $U = 0$  and  $U = 4$  eV for both symmetries cubic  $Fd\bar{3}m$  and monoclinic  $P2/c$  is plotted. The calculation details were presented in [M1,M2].

The electronic DOS calculated for the cubic structure shows similar properties, independently on  $U$ . In agreement with the previous calculations [101, 67, 102], the ground state is metallic with the minority  $t_{2g}$ -Fe( $B$ ) states at  $E_F$ . On the Fe( $A$ ) atoms all the down-spin  $3d$  states are occupied and the up-spin states lie above  $E_F$ , so these electrons do not participate in the charge transport. The antiparallel orientation of spins at the  $A$  and  $B$  sites explains the ferrimagnetic order observed in magnetite. For  $U = 4$  eV the DOS just above  $E_F$  decreases because of partial localization of electrons, however, the realistic value of  $U$  does not yet generates the insulating state. The calculations performed for the monoclinic symmetry with  $U = 0$  give very similar electron DOS as for the cubic structure.

The situation changes when the monoclinic phase is optimized at  $U > 0$ . In this case, the gap opens between the occupied  $t_{2g}$  states at the  $B1$  and  $B4$  sites and the empty states at the  $B2$  and  $B3$  ones. It corresponds to the CO with the higher density of electrons at the  $B1$  and  $B4$  sites (charge +2.4) and the lower electron occupation at the  $B2$  and  $B3$  sites (charge +2.6). Additionally, the occupied states at the  $B1$  and  $B4$  sites exhibit the antiferro-orbital ordering. The electrons at Fe( $B1$ ) occupy only the orthogonal  $d_{xz}$  and  $d_{yz}$  orbitals, while at Fe( $B4$ ) they fill the  $d_{x^2-y^2}$  states.

### 3.4 Lattice dynamics

Phonon spectrum in magnetite has been studied using various experimental techniques including the INS [103], Raman [104, 105, 106] and infrared [105] spectroscopy, as well as the nuclear inelastic scattering (NIS) [107, 108]. Temperature dependent measurements revealed significant changes of phonon frequencies at  $T_V$  indicating the participation of lattice in the mechanism of the VT [105, 106, 108]. The phonon DOS calculated for the cubic symmetry by the *ab initio*

methods shows a good agreement with the NIS spectrum [107, 108]. In [M1], we included the local Coulomb interactions for phonon calculations and a detailed comparison between the theory and experiment was done in [M2].

We have calculated the phonon spectra for fully optimized crystal structures. The obtained lattice constants are equal  $a = 8.37 \text{ \AA}$  ( $U = 0$ ) and  $8.44 \text{ \AA}$  ( $U = 4 \text{ eV}$ ), both in good agreement with the experimental value  $a_{exp} = 8.39 \text{ \AA}$ . The larger volume for  $U = 4 \text{ eV}$  stems from the increased repulsion between the  $3d$  electrons. In the  $\Gamma$  point, there are 39 optic modes classified according to the IRs of the cubic symmetry group,

$$\Gamma = A_{1g} + 2A_{2u} + E_g + 2E_u + T_{1g} + 3T_{2g} + 4T_{1u} + 2T_{2u}. \quad (9)$$

There are four infrared modes with  $T_{1u}$  symmetry, five Raman modes with  $A_{1g}$ ,  $T_{2g}$ , and  $E_g$  symmetries, and seven silent modes of  $A_{2u}$ ,  $T_{1g}$ ,  $E_u$ , and  $T_{2u}$  IRs. In Table 1, we compare the energies of the optic modes in the  $\Gamma$  point calculated at  $U = 0$  and  $U = 4 \text{ eV}$  ( $J = 0.8 \text{ eV}$ ) with the experimental data from the neutron, infrared, and Raman measurements. Apart from one infrared mode, all energies increase for nonzero  $U$ , and the largest changes reaches 20-30%. The strongest changes induced by  $U$  are found for the Raman active and in most cases it leads to better agreement with the experiment. In particular, the energy of the  $E_g$  mode, which increases by 8.9 eV, agrees better with the Raman scattering. The improvement with the experiment is found also for the highest Raman  $A_{1g}$  mode. Interestingly, these two modes, which were classified as the secondary OPs, exhibit the largest energy shifts and anomalous linewidths close to the  $T_V$ , [105, 106]. In contrast, the infrared modes have a weaker dependence on  $U$  and no significant changes were detected at  $T_V$  [105].

Table 1: Phonon energies (in meV) at the  $\Gamma$  point compared with the experimental data from Refs. [103]<sup>a</sup>, [104]<sup>b</sup>, c[105]<sup>c</sup>, and [106]<sup>d</sup>. The energy change  $\Delta E$  is given in %.

$\Gamma$	active	$U = 0$	$U = 4.0 \text{ eV}$	$\Delta E$	Experiment
$T_{2u}$		16.84	17.68	5.0	18.5 <sup>a</sup>
$T_{1u}$	I	19.98	21.46	7.4	12 <sup>b</sup>
$E_u$		21.10	22.71	7.0	
$T_{2g}$	R	24.16	25.77	6.7	23.93 <sup>c</sup> , 23.93 <sup>d</sup>
$E_g$	R	32.87	41.76	27.0	39.43 <sup>b</sup> , 38.19 <sup>c</sup> , 37.20 <sup>d</sup>
$T_{1g}$		33.10	39.27	18.6	
$A_{2u}$		35.53	38.08	7.2	
$T_{1u}$	I	38.31	40.10	4.7	32 <sup>b</sup>
$T_{1u}$	I	40.03	42.85	7.0	42.5 <sup>b</sup> , 43.4 <sup>c</sup>
$T_{2u}$		42.72	45.31	6.1	
$T_{2g}$	R	49.61	55.22	11.3	50.83 <sup>b</sup> , 50.83 <sup>d</sup>
$E_u$		52.50	54.30	3.4	
$T_{2g}$	R	65.10	68.89	5.8	67.20 <sup>b</sup> , 66.95 <sup>c</sup> , 66.95 <sup>d</sup>
$T_{1u}$	I	66.77	66.24	0.8	68 <sup>b</sup> , 69.43 <sup>c</sup>
$A_{1g}$	R	73.06	82.74	13.2	83.32 <sup>b</sup> , 83.07 <sup>c</sup> , 82.95 <sup>d</sup>
$A_{2u}$		74.21	81.33	9.6	

The phonon energies increase in spite of the larger crystal volume and interatomic distances induced by the electron repulsion. The Hubbard interaction  $U$  influences the occupation of the  $t_{2g}$  orbitals and their polarization leads to stronger localization. Thus, the charge redistribution

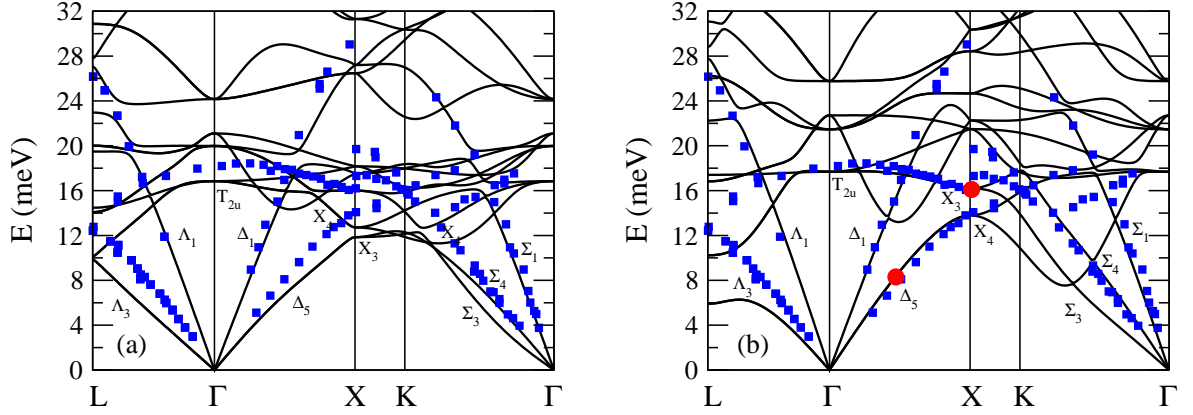


Figure 2: Phonon dispersion relations as obtained for the cubic phase of  $\text{Fe}_3\text{O}_4$  with (a)  $U = J = 0$ , and (b)  $U = 4.0$  eV and  $J = 0.8$  eV. The squares show the experimental data obtained by neutron scattering [103]. Two primary OPs  $\Delta_5$  and  $X_3$  are marked by circles in (b).

modifies screening of Coulomb interactions and the interatomic forces. More localized electrons reduce the screening of ionic interactions, and enhance the interatomic forces. This mechanism explains observed changes in the phonon spectrum, in particular, the increase of phonon energies for  $U > 0$ .

Phonon dispersion curves were calculated along the high symmetry directions ( $\Delta[001]$ ,  $\Sigma[110]$ , and  $\Lambda[111]$ ) (Fig. 2). They are compared with the low-energy phonon branches obtained by the INS [103]. Two panels in Fig. 2 show the results of calculations for  $U = 0$  (left) and for  $U = 4$  eV (right). In both cases, the energies of the longitudinal acoustic (LA) branches agree with the experiment very well, almost independently on  $U$ . It demonstrates that the LA modes do not couple strongly to electrons, and are not so sensitive to the changes in the electronic structure. Different behavior is observed for the transverse acoustic (TA) and optic (TO) modes. Along the  $\Delta$  direction, the energies of the TA phonons increase and they agreement with the neutron data improve. Analyzing the lowest optic branches in this direction, we observe also a significant changes in dispersion curves. According to the experimental assignment, the lowest mode at the  $\mathbf{k}_x$  point has the  $X_4$  symmetry, and it does not agree with calculations for  $U = 0$ . The correct sequence of phonons is achieved when electron interactions are included, so the lowest TA and TO modes get the appropriate symmetries,  $X_4$  and  $X_3$ , respectively. This result indicate that phonons at the zone boundary strongly interact with electrons, and the changes in the electronic structure induced by  $U$  significantly modify their spectrum.

### 3.5 Mechanism of the Verwey transition

The group theory analysis revealed that the Verwey transition is induced by two OPs  $\Delta_5$  and  $X_3$ . The computational studies confirmed that these two modes strongly couple to electrons, and this coupling is considerably enhanced by the Hubbard interaction  $U$  [**M1,M2**]. We studied how the crystal structure and the electronic DOS change due to lattice distortion generated by the polarization vectors, calculated by the PHONON program. In Fig. 3, we present the dependence of the total energy of crystal on the amplitude of the normal modes. For  $U = 0$ , the deformation of the crystal, induced by any of the considered modes, always leads to larger energy. It means that the cubic phase without electron correlations is the absolute ground state, and its energy cannot be lowered by crystal deformation. The character of the electron-phonon coupling changes when

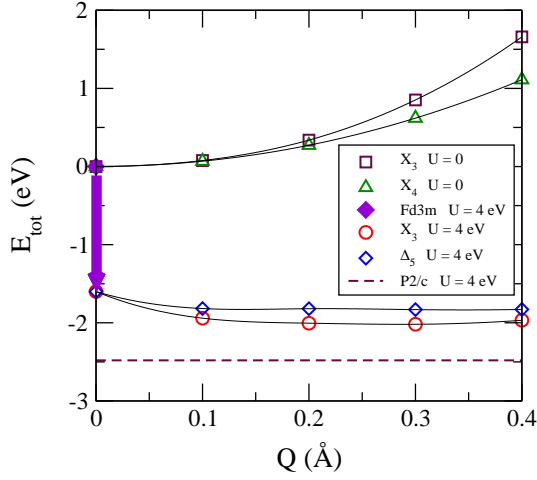


Figure 3: Total energy of  $\text{Fe}_3\text{O}_4$  as a function of the phonon amplitude  $Q$  of the  $X_3$ ,  $X_4$ , and  $\Delta_5$  modes for  $U = 0$  and  $U = 4$  eV. The arrow indicates the energy gain  $\Delta E \sim 1.6$  eV due to the orbital polarization.

the local interaction  $U$  is included. It induces polarization of the  $t_{2g}$  orbitals and their partial ordering. In Fig. 3, the gain in energy  $\Delta E \sim 1.6$  eV due to orbital polarization is illustrated by the arrow starting at  $E = 0$ . This orbital order, however, has no long-range character and it does not induce yet the metal-insulator transition. It has to be stabilized by the electron-phonon coupling, which leads to further decrease in energy. We found that for  $U = 4$  eV both phonon OPs:  $X_3$  and  $\Delta_5$  lower the total energy (see Fig. 3).

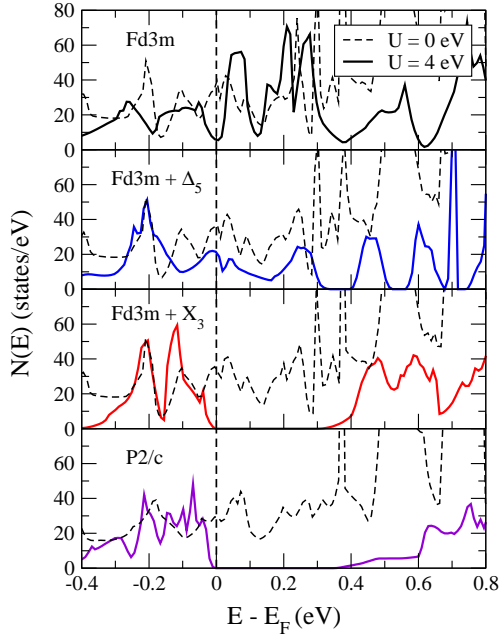


Figure 4: Electronic DOSs for the  $Fd\bar{3}m$ ,  $Fd\bar{3}m + X_3$ ,  $Fd\bar{3}m + \Delta_5$ , and  $P2/c$  symmetry for  $U = 0$  (dashed line)  $U = 4$  eV (solid line).

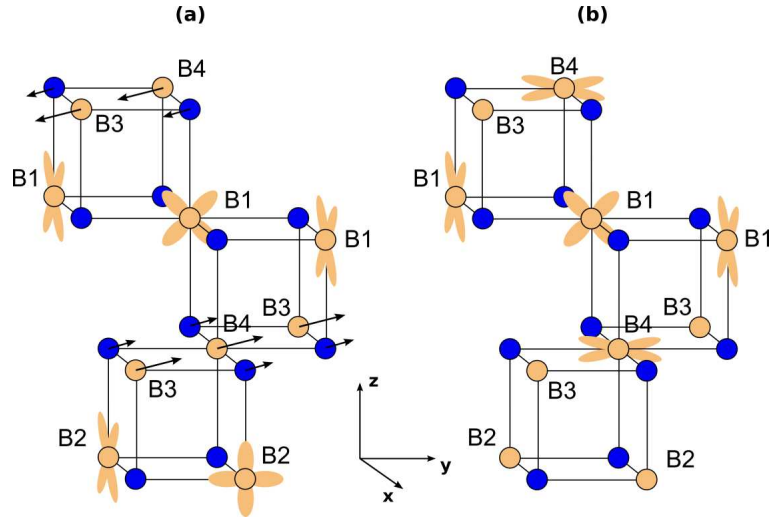


Figure 5: Orbital order on the Fe(*B*) ions induced by (a) the  $X_3$  phonon (black arrows) and (b) the  $P2/c$  monoclinic distortion.

The effect of both phonons on the electronic structure for  $U = 0$  and  $U = 4$  eV is presented in Fig. 4, where DOSs of the distorted crystals are compared with the cubic phase. For the  $\Delta_5$  mode, magnetite remains a metal, although at  $U = 4$  eV, a significant reduction of the spectral weight above  $E_F$  is caused by the electron-phonon interaction. This coupling is stronger for the  $X_3$  phonon, which at  $U = 4$  eV, opens the gap at  $E_F$  leading to the metal-insulator transition. The insulating gap  $\Delta = 0.3$  eV is comparable with the experimental value (0.15 eV) [109] and the value found for the  $P2/c$  structure (the bottom panel of Fig. 4).

The displacement of atoms in the  $X_3$  mode are plotted in Fig. 5(a). The Fe(*B*) and O atoms move parallelly along the [110] directions; oxygen displacements are about 30% smaller than the iron ones. The atom movement in a single plane modulates the Fe-O distances in perpendicular direction and generates the orbital ordering in the nearest neighbor planes. The electrons occupy the orthogonal  $d_{yz}$  and  $d_{xz}$  orbitals on the Fe(*B*) atoms, thus forming the antiferro-orbital order. The splitting of the  $t_{2g}$  states by the  $X_3$  mode generates also the fractional charge ordering. It is consistent with the charge-orbital order found in the  $P2/c$  structure, Fig. 5(b), although, more complex configuration of charges and orbitals in the monoclinic phase results from the condensation of two OPs:  $X_3$  and  $\Delta_5$ . The latter is responsible for the doubling of the unit cell in the  $c$  direction, so the  $2a$  modulation of the charge-orbital pattern results from the electron-phonon coupling at the  $\mathbf{k}_\Delta$  point.

In this picture, the OPs are composed of the lattice components, the  $\Delta_5$  and  $X_3$  phonons, and the corresponding electronic parts. The condensation of the OPs means the simultaneous breaking of the crystal symmetry and the charge-orbital ordering. Therefore, instead of a typical soft-mode behavior, the critical fluctuations of charge density coupled to lattice distortions were observed by the diffuse scattering. As discussed earlier, the cooperation of two OPs  $X_3$  and  $\Delta_5$  is the essence of the VT. The  $X_3$  mode is responsible for the metal-insulator transition, leading to the charge-orbital ordering. The  $\Delta_5$  phonon alone does not generate the insulating state but it induces the crystal distortion at  $\mathbf{k}_\Delta$ , thus, it is crucial for the monoclinic distortion. The theory based on two OPs, therefore, joins the two main concepts of the VT, charge ordering and crystal distortion, in one coherent scenario.

The presented theory explains the majority of experimental facts related to the VT, but a few

open problems remain. One of them is the exact crystal structure below the transition, which has not been completely resolved yet. The monoclinic  $P2/c$  space group used in our analysis describes the low-temperature phase very well [88], but there are additional tiny distortions, which lowers crystal symmetry to the space group  $Cc$ . There is also ongoing discussion on the magnitude of the charge-orbital ordering below  $T_V$  [110]. Another problem concerns the behavior of magnetite at high pressures. It was observed that the critical temperature  $T_V$  decreases under pressure and drops to zero around  $p = 8$  GPa [111]. It is not clear if the same mechanism drives the VT at high pressures, and how it is modified by the quantum critical point discussed in a recent work [112]. One more open question concerns the VT in the doped and non-stoichiometric systems. In particular, the observed change of the transition character, from the first order to second order, at small doping, is still not well understood [113].

## 4 Phonons in the actinide compounds

### 4.1 Unconventional superconductivity in PuCoGa<sub>5</sub>

Discovered in 2002, PuCoGa<sub>5</sub> is the first superconductor containing Pu with the critical temperature  $T_c = 18.5$  K [114], the highest among all known  $f$ -electron compounds. In the heavy-fermion superconductors, like CeCoIn<sub>5</sub> or UPt<sub>3</sub>,  $T_c$  does not exceed 3 K. PuCoGa<sub>5</sub> is a strongly type II superconductor with the high upper critical field  $H_{c2}(T = 0) = 740$  kOe, the coherence length  $\xi = 2.1$  nm, and the Ginzburg-Landau parameter  $\kappa = 32$ . There is no evidence of a long-range magnetic order, however, the Curie-Weiss behavior of the magnetic susceptibility above  $T_c$  indicates the existence of disordered local moments on Pu. The crystal structure is tetragonal with the  $P4/mmm$  space group consisting of the Pu-Ga planes separated by the Co and Ga layers (see Fig. 6). There are two nonequivalent positions of gallium, one at the basal plane Ga<sub>I</sub>(0.5,0.5,0) and second at Ga<sub>II</sub>(0.5,0,z). Co atom is located at half distance between two Pu atoms in the  $c$  directions.

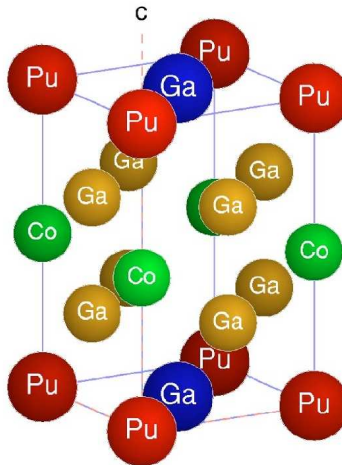


Figure 6: Crystal structure of PuCoGa<sub>5</sub>.

The electronic structure of PuCoGa<sub>5</sub> was studied by the DFT methods [115, 116, 117] as well as the photoemission spectroscopy [118]. The states close to  $E_F$  are dominated by the  $5f$  electrons, with small contribution of the  $d$  and  $p$  states. In the LDA, the  $5f$  electrons are completely delocalized with the maximum in DOS at  $E_F$  [115]. It does not agree with the photoemission spectrum consisting of a small peak at  $E_F$  and the main spectral weight shifted to lower energies by about 1.2 eV. Much better agreement is found in the spin-polarized LDA [119] or LDA+ $U$  calculations [120]. The local Coulomb interaction reduces further the intensity at  $E_F$  and shifts the main manifold to lower energies 1-2 eV (see Fig. 7). Electron correlations beyond the static approximation were included in the DMFT studies [121]. These correlations contribute to the narrow peak at  $E_F$  and suppress the long-range magnetic order, thus improving the agreement with the experiment.

Similarity to the heavy-fermion superconductors [122] and strong electron correlations point out to the possibility of unconventional, magnetically mediated mechanism of superconductivity. The temperature dependence of resistivity is consistent with the spin fluctuation model [123]. The spin susceptibility and the spin-lattice relaxation rate indicate the  $d$ -wave gap function [124]. On the other hand, the observed  $T_c$  is within the range of standard electron-phonon mechanism

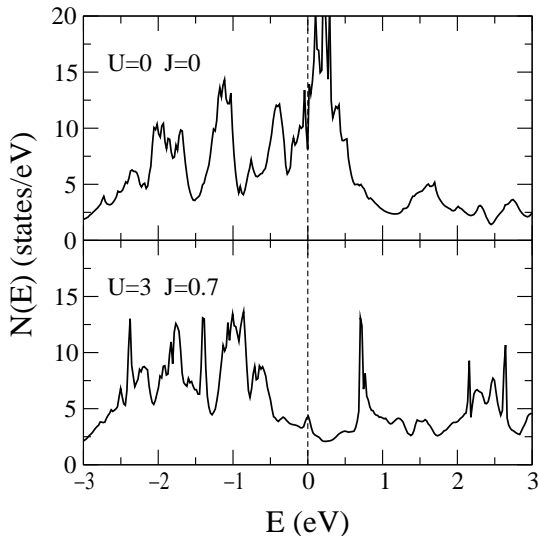


Figure 7: The total electron DOS of PuCoGa<sub>5</sub> for the NM ( $U = 0$ ) and FM ( $U = 3$  eV) states.

of superconductivity. Some discrepancy between the phonon model and the experimental data, discussed in [123], may result from applying the simplified Einstein model.

The realistic model of superconductivity requires the information on the phonon spectrum. The main objective of our studies was to calculate the phonon spectrum and to investigate how the local Coulomb interaction  $U$  influences the lattice dynamics in PuCoGa<sub>5</sub>. We have calculated the phonon dispersion curves using the GGA+ $U$  approach, and found a strong dependence of the phonon energies on the local Coulomb interaction  $U$ . This result was then verified experimentally using the inelastic x-ray scattering at the European Synchrotron Radiation Facility (ESRF) in Grenoble. The main results of the theoretical and experimental studies, presented in three articles [P1,P2,P3], are described in the following sections.

## 4.2 Electron correlations and phonons in PuCoGa<sub>5</sub>

We optimized the crystal and electronic structure of PuCoGa<sub>5</sub> using the total-energy DFT method. The calculations were performed in the  $2 \times 2 \times 1$  supercell with 28 atoms. We considered the nonmagnetic (NM) state with  $U = J = 0$ , and two magnetic AF and FM long-range orders with  $U = 3$  eV and  $J = 0.7$  eV. The obtained crystal parameters are compared with the experimental data in Tab. 2. For the NM state the lattice constants are underestimated due to the lack of magnetic interactions. The agreement with the experiment improves in the magnetically ordered states, and the lattice parameters have similar values for the AF and FM configurations. Although, the long-range magnetic order in PuCoGa<sub>5</sub> does not exist, this result indicates that

Table 2: Lattice constants  $a$  and  $c$  (in Å) and the internal Ga coordinate  $z$ .

	NM ( $U = 0$ )	FM ( $U = 3$ eV)	AF ( $U = 3$ eV)	exp (Ref. [114])
$a$	4.197	4.246	4.249	4.232
$c$	6.693	6.917	6.883	6.786
$z$	0.304	0.311	0.312	0.312

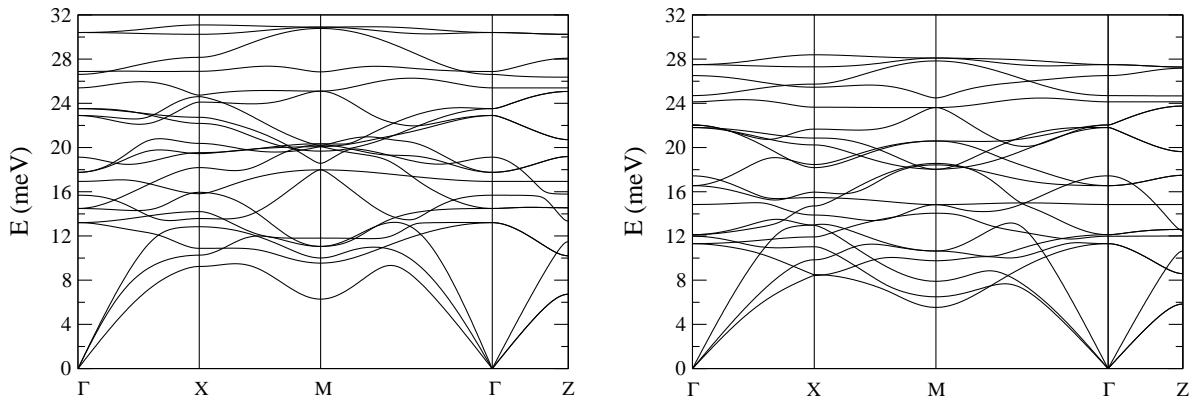


Figure 8: Phonon dispersion curves of PuCoGa<sub>5</sub> for  $U = 0$  (left) and  $U = 3$  eV (right).

local magnetic interactions influence the crystal parameters. Similarly, the electronic DOS obtained for  $U = 3$  eV shows much better agreement with the photoemission spectrum. In Fig. 7, we compare the results of our calculations for the NM and FM state. In the latter case, the main  $5f$ -electron peak is shifted from the Fermi level to lower energies  $E \sim -1$  eV.

We have calculated the phonon dispersion curves for both the NM and FM ground states, with the corresponding optimized crystal structures. The HF forces were calculated from the independent atomic displacements ( $u = 0.02$  Å) of all nonequivalent atoms: two for Pu, Co, and Ga<sub>I</sub> (along  $x$  and  $z$ ) and three for Ga<sub>II</sub> (along  $x$ ,  $y$ , and  $z$ ). In the zone-center (the  $\Gamma$  point), there are eighteen optic modes, classified according to the following irreducible representations:

$$\Gamma = A_{1g} + B_{1g} + 2E_g + 3A_{2u} + B_{2u} + 4E_u. \quad (10)$$

The phonon energies and polarization vectors at the  $\Gamma$  point are analyzed in details in [P1]. The energies of all modes depend on Coulomb interaction  $U$ , and the largest changes ( $\sim 30\%$ ) were found for the two lowest optic modes  $A_{2u}$  and  $E_u$ . It follows mainly from the modified geometry of the crystal for finite  $U$  and the modified  $f$ -electron charge distribution. In fact, these two mechanisms give opposite effects. On one hand, the increase of the interatomic distances due to larger Coulomb repulsion leads to the reduction of the force constants and phonon energies. On the other hand, a stronger electron localization weakens the charge screening and enhances the force constants. In PuCoGa<sub>5</sub>, the first effect is dominating, and all phonon energies decreases with  $U$ . Fig. 8 presents the comparison between the phonon dispersion curves calculated for  $U = 0$  (left) and  $U = 3$  eV (right). Apart from an overall softening of phonon energies, there are also qualitative changes in the dispersion curves. This is clearly seen for the lowest TA mode, which is separated from other modes for  $U = 0$ , while for  $U = 3$  eV it intersects with other phonons close to the  $X$  and  $M$  points.

In order to verify the obtained results and to find out which case,  $U = 0$  or  $U = 3$  eV, better describes a real material, we have measured the phonon dispersion curves using the IXS. This technique was chosen, because the single crystal size of PuCoGa<sub>5</sub> was too small for the INS. The experiment was carried out on the beamline ID28 at the ESRF in collaboration with the group of physicists from Grenoble (ESRF,CEA) and from the Japan Atomic Energy Agency in Tokai. The <sup>242</sup>Pu-based samples were prepared in the Institute for Transuranium Elements in Karlsruhe, and encapsulated in order to comply with safety regulations. The measuring of phonon branches was guided by the calculations of the neutron scattering intensity using the PHONON program. The details of the experimental setup are described in [P2].

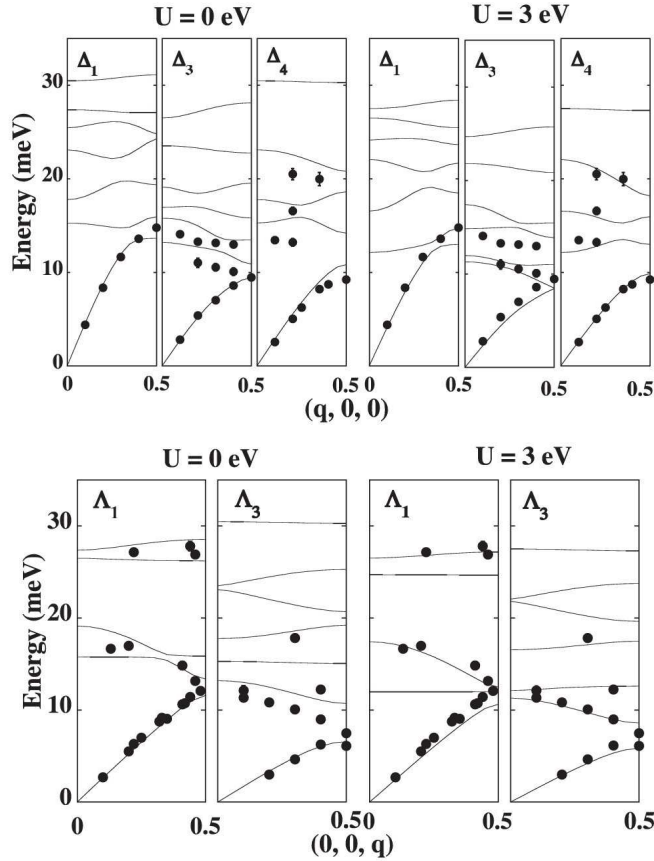


Figure 9: Phonon dispersion curves of PuCoGa<sub>5</sub> in the  $\Delta$  [100] (top) and  $\Lambda$  [001] direction (bottom) compared with the IXS experimental points.

The comparison between the theory and experiment is presented in Fig. 9, where dispersions are plotted in separate groups classified according to their irreducible representations. In the upper part, there are dispersions along the [100] direction. The longitudinal modes correspond to the  $\Delta_1$  symmetry, and the transverse modes belong to the  $\Delta_3$  and  $\Delta_4$  representations. The representation  $\Delta_3$  contains the transverse modes with polarization along the  $c$  axis and the  $\Delta_4$  one phonons polarized along the  $b$  axis. All acoustic modes (independently on  $U$ ) agree very well with the experiment. They are less sensitive to changes in lattice geometry than the optic ones. All LO modes show significant dependence on  $U$ , but they were not measured in the [100] direction. For the TO modes,  $\Delta_3$  and  $\Delta_4$ , there is a systematic improvement connected with the softening of these modes. Especially, the lowest TO modes strongly depend on  $U$ , and their energies approach the experimental values.

Along the [001] direction, the changes induced by electron correlations have similar character. Among the LO modes, with the  $\Lambda_1$  symmetry, the largest shift is found for the lowest mode, from 15.8 meV to 12 meV (this mode was not measured). Two other LO modes calculated for  $U = 3$  eV agree very well with the experimental points. The transverse modes ( $\Lambda_3$ ) are doubly degenerated with two equivalent polarizations along the  $a$  and  $b$  directions. The two lowest TO modes strongly soften with  $U$  and the agreement with experiment is significantly improved. A strong shift is also visible for the highest mode, which changes its energy from 30.5 to 27.5 meV.

The observed softening of phonon energies results from changes in the force constants  $\Phi_{\alpha\beta}$

induced by Coulomb interactions (see [P3]). The largest changes were found for the Pu and Ga atoms located in the Pu-Ga plane. Both the on-site force constants  $\Phi_{xx}$  and  $\Phi_{zz}$  for these atoms show significant decrease for  $U = 3$  eV. For example,  $\Phi_{zz}$  for Ga changes from 4.04 to 1.5 eV/Å<sup>2</sup>. The changes induced by  $U$  are visible also in the total and partial phonon DOS's plotted in Fig. 10. The low-energy range of phonon spectrum is mainly modified by the vibrations of Ga atoms. Their masses are much lower than those of the Pu atoms, and their movement is more sensitive to changes in the crystal geometry. The Pu partial DOS is mainly modified in the middle range of energies. At higher energies, the changes are mainly caused by the Ga and Co atoms.

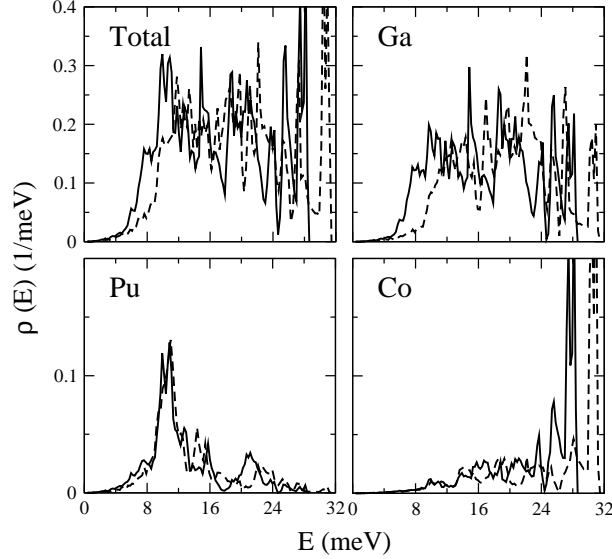


Figure 10: The total and partial phonon DOSs of PuCoGa<sub>5</sub> for  $U = 0$  (dashed line) and  $U = 3$  eV (solid line).

### 4.3 Electron-phonon interaction

Having the phonon energy spectrum, we calculated the critical temperature  $T_c$  of the superconducting state, using the Allen-Dynes formula [125]

$$k_B T_c = \frac{\langle \omega \rangle}{1.20} \exp \left\{ - \frac{1.04(1 + \lambda)}{\lambda - \mu^*(1 + 0.62\lambda)} \right\}, \quad (11)$$

where  $\langle \omega \rangle$  is the average phonon energy,  $\lambda$  is the electron-phonon coupling constant, and  $\mu^*$  is the value of the effective Coulomb interaction. The coupling constant  $\lambda$  was estimated taking only phonons at the  $\Gamma$  point. For each mode  $\nu$ ,  $\lambda_\nu$  was calculated using the following formula [126]

$$\lambda_\nu = \frac{N(E_F) \langle g_\nu^2 \rangle_{E_F}}{\omega_\nu^2}. \quad (12)$$

The electron-phonon matrix element is given by

$$g_{\nu; k, n} = \sum_{\alpha} \frac{e_{\alpha}^{\nu}}{\sqrt{M_{\alpha}}} \langle k, n | \nabla_{\alpha} V | k, n \rangle, \quad (13)$$

where  $\alpha$  runs over all atoms and directions in the unit cell,  $e_{\alpha}^{\nu}$  are the polarization vectors, and  $\nabla_{\alpha} V$  is the change of potential associated with atom displacement  $u_{\alpha}$ . Diagonal matrix elements

in Eq. (13) can be obtained from the deformation potential for the state  $|k, n\rangle$  [127]

$$\langle k, n | \nabla_{\alpha} V | k, n \rangle = \frac{\partial \epsilon_{kn}}{\partial u_{\alpha}}, \quad (14)$$

where  $\epsilon_{kn}$  are electron energies near the Fermi level. Since the average phonon energy is weakly dependent on  $U$ , we take only values for  $U = 0$ . For the obtained  $\lambda \sim 0.7$  and  $\langle \omega \rangle = 212$  K, we get the  $T_c = 14$  K (at  $\mu^* = 0$ ). For  $\mu^* = 0.1$ , this value is reduced to  $T_c = 7$  K. The obtained values are lower than the observed  $T_c = 18$  K, however, the method used here is very approximate and does not take into account possible strong electron-phonon effects for  $\mathbf{k} \neq 0$ .

Recently, the phonon-mediated pairing mechanism was studied within the Eliashberg theory [128]. The authors used the phonon DOS calculated in [P1] (Fig. 10) to obtain the electron-phonon spectral function  $\alpha F(\omega)$ . Additionally, the  $d$ -wave pairing symmetry consistent with the experimental observation [124] was assumed. The temperature dependence of the superconducting gap  $\Delta(T)$  and electrical resistivity of PuCoGa<sub>5</sub> was calculated and very good agreement with the experiment was found. This result supports the view that phonons may be responsible for the superconductivity in PuCoGa<sub>5</sub>. Moreover, a strong influence of electron correlations on lattice dynamics discussed in the previous sections suggests a possible interplay of the magnetic and phononic degrees of freedom in such mechanism. One of the important question arises: why only the plutonium compound in the series ACoGa<sub>5</sub> with  $A = \text{U, Np, Pu, and Am}$  is superconducting. The results on lattice dynamics of UCoGa<sub>5</sub>, presented in the next section, shed some light on this issue.

#### 4.4 Phonons in UCoGa<sub>5</sub>

UCoGa<sub>5</sub> is isostructural to PuCoGa<sub>5</sub> and belongs to a large group of UTGa<sub>5</sub> compounds, where T is a transition metal. In contrast to PuCoGa<sub>5</sub>, UCoGa<sub>5</sub> is a nonsuperconducting, temperature-independent paramagnet, with much lower specific heat coefficient  $\gamma = 5$  mJ/mol K<sup>2</sup>. These features indicate the itinerant character of  $5f$  electrons [129], supported also by the *ab initio* studies [115, 130]. The  $5f$  electrons dominate at the Fermi level, however, the majority of the  $5f$  states are unoccupied and shifted to higher energies. The position of the  $5f$  band makes the electronic properties of UCoGa<sub>5</sub> significantly different than those of PuCoGa<sub>5</sub>. The calculated Fermi surface and the electronic spectrum show good agreement with the de Haas-van Alphen experiment [129] and the x-ray photoemission measurement [131].

We optimized the electronic and crystal structure of UCoGa<sub>5</sub> using the GGA approach ( $U = 0$ ). The details of calculations are presented in [U1]. The obtained lattice parameters  $a = 4.240$  Å,  $c = 6.708$  Å, and  $z = 0.306$ , agree very well with the experimental values  $a = 4.234$  Å,  $c = 6.723$  Å, and  $z = 0.305$ . The HF forces and force constants were calculated by displacing all nonequivalent atoms from their equilibrium positions by 0.03 Å. The phonon dispersion curves along high-symmetry directions are presented in Fig. 11. They are compared with the experimental points measured at room temperature by the INS carried out on the triple axes spectrometers TAS-1 and TAS-2 at the reactor JRR-3 in JAERI (Japan). Apart from the vicinity of the  $M$  point, the agreement with the measured acoustic and optic modes is very good. At the  $M$  point, the lowest TA mode could not be measured due to a very low intensity of neutron scattering. The second lowest mode is shifted about 2 meV comparing to the measured value.

The presented result was obtained without including the Hubbard interaction  $U$ . The calculations with the same values of  $U = 3$  eV and  $J = 0.7$  eV as for PuCoGa<sub>5</sub> in the magnetically polarized state were unstable and we could not get good convergence while optimizing the electronic structure. It confirms the non-magnetic itinerant character of  $5f$  electrons in this compound. While PuCoGa<sub>5</sub> and UCoGa<sub>5</sub> have identical crystal structures and very similar

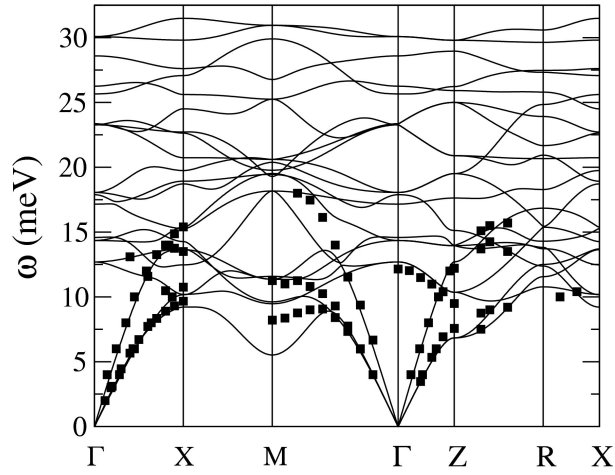


Figure 11: Phonon dispersion curves of  $\text{UCoGa}_5$  compared with the experimental points obtained by the neutron scattering.

lattice parameters, the difference in lattice dynamics in these compounds results from different electronic properties. In the U compound, the  $5f$  electrons exhibit the itinerant character, while they are partially localized in the Pu compound. This is the origin of significantly different properties of these two materials.

## 5 Lattice dynamics of Eu

Europium occupies rather exceptional position among the lanthanides. It is the only RE which crystallizes in the body-centered cubic structure in normal conditions. Eu exhibits a large atomic volume due to its divalent valency. The  $4f$  shell is half-filled with the expected maximum magnetic moment  $7\mu_B$  and the orbital moment equal zero. The crystal field interactions reduce this moment to  $5.9\mu_B$ . At  $T_N = 91$  K, Eu undergoes a transition to the AF state with the incommensurate spin spiral order with the period  $3.6a$  [132]. The optimized lattice constant obtained in the standard DFT calculations is a few percent smaller than the experimental value [133]. This overbinding of the  $4f$  electrons can be weakened by applying the self-interaction correction [55] or the LDA+ $U$  method [134].

Our calculations were performed in the  $2 \times 2 \times 2$  supercell with 16 atoms. We assumed the FM ground state, which gives after minimization the magnetic moment  $7.1\mu_B$ . The lattice constant  $a = 4.432$  Å is smaller about 2.7% than the measured value  $a = 4.555$  Å at 100 K. The HF forces were calculated by displacing the Eu atom in one of the main directions by  $u = 0.07$  Å. In Fig. 12(a), the phonon dispersions are plotted along the high-symmetry directions between the  $\Gamma = (0,0,0)$ ,  $N = (\frac{1}{2}, \frac{1}{2}, 0)$ ,  $P = (\frac{1}{2}, \frac{1}{2}, \frac{1}{2})$  and  $H = (0,0,1)$  points. All phonon branches are positive, although, because of a large atomic mass of Eu, the phonon energies are very low  $E < 10.5$  meV.

The phonon DOS is plotted in Fig. 12(b). By comparing the phonon DOS with the dispersion curves one can easily identify the three peaks. The peak at 5 meV corresponds to the lowest TA mode observed between the  $P$  and  $H$  points. A sharp peak at 7.5 meV results from a flat mode found in the  $NP$  direction. The highest mode around 10 meV corresponds to vibrations along the  $NH$  direction. The observed shoulder at 3 meV is associated with a low-lying TA mode at the  $N$  point.

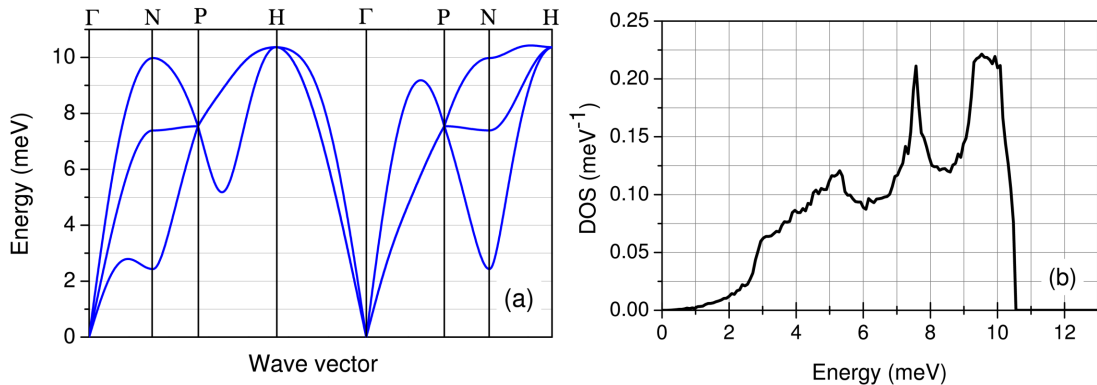


Figure 12: Phonon dispersion curves (a) and phonon DOS (b) of Eu.

The phonon spectrum of Eu was measured by the nuclear inelastic scattering method. This technique uses the resonant nuclear absorption, characteristic for the Mössbauer isotopes such as  $^{57}\text{Fe}$  and  $^{119}\text{Sn}$  [135]. The phonon spectra are obtained by measuring the intensity of phonon creation or annihilation as a function of difference between the incident radiation energy and the nuclear resonance. Besides Eu, this technique was used to study phonons in  $^{161}\text{Dy}$  [136]. The Eu experiment was performed at the ID22 beamline of the ESRF in Grenoble. For measurements, the 200-nm-thick epitaxial film was prepared and investigated *in situ* in ultra-high vacuum conditions. Details of the sample preparation and the experimental set-up are described in [E1]. The obtained phonon DOS at  $T = 100$  K is presented in Fig. 13. A three-peak structure is very well

resolved in spite of the instrumental broadening of the peaks. To compare this spectrum with the theory, we have convoluted the calculated DOS with a Gaussian function taking the width at half maximum of 1.45 meV (the experimental resolution). The intensities and energies of the peaks agree very well with the measured data. The additional small peak at 13 meV is not accounted for by the calculations and most likely it arises due to the adsorption of atoms from the residual gases. We have compared also the theoretical and experimental values of the specific heat ( $C_{ph}$ ), vibrational entropy ( $S_{ph}$ ), mean atomic displacements ( $u_{av}$ ) and force constants ( $\Phi_{av}$ ), as well as the sound velocity ( $v_T$ ) at  $T = 100$  K finding a perfect agreement between them (see Tab. 3).

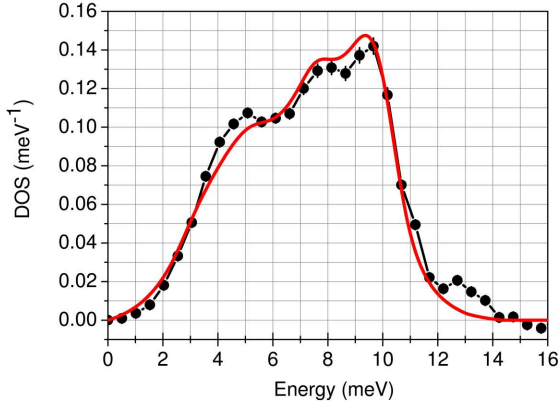


Figure 13: The comparison of the theoretical phonon DOS (solid line) with the experimental NIS data (points) for the bcc phase of Eu.

For europium, we did not study the effect of local Coulomb interactions on phonons. Previous calculations demonstrated that the Hubbard interaction  $U$  changes the position of the  $4f$  band below the Fermi level and increases the crystal volume [133, 134]. We expect some modification of the phonon spectrum due to stronger electron localization and crystal expansion. However, a very good agreement between the calculated DOS for  $U = 0$  and the experiment indicates that the interatomic forces are reproduced very well and the effect of electron correlations on phonons is not significant. It confirms that the  $4f$  electrons in lanthanides are much more localized than the  $5f$  electrons in actinides and do not play the active role in the interatomic bonding. Nevertheless, the influence of electron correlations on phonons in the RE materials is an open problem and will be the subject of future studies.

Table 3: Thermodynamic and elastic properties of Eu at 100 K obtained from the experimental and theoretical phonon DOS. The systematic errors are indicated in brackets.

physical quantity	experiment	theory
$C_{ph}$ ( $k_B/\text{atom}$ )	2.8(1)	2.8
$S_{ph}$ ( $k_B/\text{atom}$ )	3.8(1)	3.8
$u_{av}$ ( $\text{\AA}$ )	0.094(2)	0.091
$\Phi_{av}$ (N/m)	33(2)	32.42
$v_T$ (m/s)	1658(30)	1639

## 6 General remarks and summary

The presented results demonstrate a strong dependence of phonon spectra and related dynamical properties on the electronic structure. We focused on the effects induced by local Hubbard-type interactions, particularly important for the transition-metal compounds and  $f$ -electron metals. Good examples are two correlated systems discussed here,  $\text{Fe}_3\text{O}_4$  and  $\text{PuCoGa}_5$ . In both cases, the phonon spectra calculated within the standard DFT approach show significant qualitative and quantitative discrepancies with the experiments. The agreement is largely improved by including the realistic values of the Hubbard interaction within the LDA+ $U$  method. Electron correlations modify also electron-phonon interactions, and in the case of magnetite, this interplay of electrons with lattice plays the crucial role in the mechanism of the Verwey transition.

In two other materials,  $\text{UCoGa}_5$  and  $\text{Eu}$ , electron correlations seem not to effect strongly phonon energies. This conclusion is based on good agreements between the experiments and calculations assuming  $U = 0$ . In the uranium compound, the  $5f$  electrons are delocalized and the Coulomb repulsion between them is strongly screened. This situation is similar to the  $d$ -electron elements like Fe or Ni, where standard DFT approach is sufficient to obtain phonon spectra. In  $\text{Eu}$ , we have the opposite situation. The  $4f$  electrons are localized in the core and do not participate in atomic bonding. However, the case of  $\text{Eu}$  is rather exceptional, so, more studies are needed for better understanding of lattice dynamics in the rare earths.

The presented examples show that the first-principles calculations can be successfully used for studying strongly correlated electron-phonon systems. Often such calculations are indispensable for planning and performing the experiments on lattice dynamics in new complex materials. In many cases, the experimental results obtained by the highly advanced techniques, like the inelastic x-ray and resonant nuclear scattering, can be understood and interpreted only by comparison with the theory.

In the following points, I summarize the main results presented in the discussed papers.

**[M1]** The mechanism of the Verwey transition in magnetite was studied using the group theory and *ab initio* methods. The local Coulomb interactions between electrons in the  $3d$  states on Fe were included within the GGA+ $U$  method. Two primary order parameters with symmetries  $X_3$  and  $\Delta_5$  were identified. These phonons strongly couple to electrons, breaking the cubic symmetry and lowering the total energy of the crystal. It was found that the  $X_3$  mode induces the metal-insulator transition for the realistic value of the Hubbard interaction  $U = 4$  eV.

**[M2]** The structural phase transition from the high-symmetry cubic to the low-symmetry monoclinic phase in magnetite was studied using the group theory. All primary and secondary order parameters were found and the Landau free energy for the Verwey transition was derived. The crystal structure parameters of both phases and phonon dispersions were studied in details using the GGA+ $U$  method. The agreement between the theory and experiment is significantly improved by including the local Coulomb interaction  $U = 4$  eV and Hund's exchange  $J = 0.8$  eV. It was revealed that phonon energies are increased due to electron localization and the electron-phonon coupling is enhanced due to the charge-orbital ordering. Both effects are induced by the Hubbard interaction  $U$  between the  $t_{2g}$  electrons on iron.

**[M3]** The Landau theory was used to study the Verwey transition in magnetite. The free energy functional was expanded in a series of components belonging to two primary order parameters  $X_3$  and  $\Delta_5$ , and one secondary order parameter  $T_{2g}$ . The conditions of simultaneous condensation of both primary order parameters resulting in the low-symmetry monoclinic phase were obtained and discussed. The temperature dependence of the elastic constant  $c_{44}$  was derived and the

mechanism of critical softening due to coupling between the shear strain and order parameters was analyzed.

**[P1]** The electronic and crystal structure of the PuCoGa<sub>5</sub> superconductor were calculated. A good agreement with the experimental data was achieved for the Coulomb repulsion  $U = 3$  eV and Hund's exchange  $J = 0.7$  eV for the  $5f$  electrons on Pu. A large influence of electron correlations on phonon dispersion curves was revealed. The softening of the transverse optical modes ( $\sim 30\%$ ) is caused by the crystal volume expansion induced by the local electron repulsion. Using the phonon density of states, the heat capacity and electron-phonon coupling constant were obtained. The possibility of phonon mechanism of superconductivity in PuCoGa<sub>5</sub> was discussed.

**[P2]** The phonon dispersion curves of PuCoGa<sub>5</sub> were measured by the inelastic x-ray scattering technique. In the experiment, the choice of the Brillouin zones, scattering wave vectors, and energy ranges was guided by the dynamical structure factor calculations. A very good agreement between the measured and theoretical dispersion curves was found for the realistic value of the Hubbard interaction  $U = 3$  eV. This result indicates a significant effect of electron correlations on lattice dynamics in PuCoGa<sub>5</sub>.

**[P3]** The influence of the on-site Hubbard interaction  $U$  on force constants  $\Phi_{\alpha\beta}$  and phonon density of states in PuCoGa<sub>5</sub> was analyzed. A small anisotropy of the force-constant matrices exists due to the tetragonal symmetry. The increase of the interatomic distances induced by the Coulomb repulsion make all force constant smaller. The largest changes were found for the Pu and Ga atoms; the on-site force constant  $\Phi_{zz}$  is reduced more than 60%, what corresponds to a large softening of the Ga partial DOS.

**[U1]** The phonon dispersion curves of UCoGa<sub>5</sub> were studied using the GGA calculations and the inelastic neutron scattering method. The calculations were performed without including the Hubbard interaction  $U$ . A good agreement between the theory and experiment supports the view that the  $5f$  electron in UCoGa<sub>5</sub> have itinerant character and correlation effects are much weaker than in the isostructural PuCoGa<sub>5</sub>.

**[E1]** The lattice dynamics of the rare-earth metal Eu was studied within the GGA method. The electronic structure, including the  $4f$  electrons, and crystal parameters were optimized for the cubic bcc phase. The calculated phonon density of states was compared with the phonon spectrum obtained by the inelastic nuclear scattering method. A very good agreement between them indicates that correlation effects in the  $4f$  states have rather small effect on phonons. The thermodynamic and elastic properties derived from the theory and experiment were successfully compared.

## Acknowledgements

I would like to express my deep gratitude to Prof. Krzysztof Parlinski for very inspiring and fruitful collaboration, for supporting my scientific activity, and creating excellent atmosphere and conditions to work in the Department of Materials Research By Computers.

I am deeply thankful to Prof. Andrzej M. Oleś for his helpful collaboration and sharing with me his knowledge on strongly correlated systems.

I am grateful to my colleagues and collaborators, Dr. Małgorzata Sternik, Dr. Jan Łażewski, and Dr. Paweł Jochym, with whom the scientific work is a great pleasure and adventure.

My gratitude goes also to all collaborators, who participated in the experimental work presented in this thesis. In particular, I would like to mention Dr. Stephane Raymond from ILL, Dr. Michael Krisch from ESRF, and Dr. Svetoslav Stankov from Karlsruhe Institute of Technology.

I would like to thank many persons, who helped me in my scientific work. My special gratitude goes to Prof. Jerzy Konior with whom I collaborated for many years, and who helped me to complete my Ph.D. thesis. I would like to thank Prof. Takeshi Egami for great collaboration during my postdoc at the University of Pennsylvania.

I am very thankful to Małgorzata Litwiniszyn, who helped me to organize all scientific activities and to prepare necessary documents for the habilitation procedure.



## References

- [1] E. Wigner and F. Seitz, Phys. Rev. **43**, 804 (1933); J. C. Slater, Phys. Rev. **51**, 846 (1937); C. Herring, Phys. Rev. **57**, 250 (1940).
- [2] D. Hartree, Proc. Cambridge Philos. Soc. **24**, 89 (1928); V. Fock, Z. Physik **61**, 126 (1930); J. C. Slater, Phys. Rev. **30**, 210 (1930).
- [3] P. Hohenberg and W. Kohn, Phys. Rev. **136**, 864 (1964).
- [4] W. Kohn and L. J. Sham, Phys. Rev. **140**, 1133 (1965).
- [5] D. C. Langreth and M. J. Mehl, Phys. Rev. B **28**, 1809 (1983); J. P. Perdew and Y. Wang, Phys. Rev. B **33**, 8800 (1986).
- [6] R. O. Jones and O. Gunnarsson, Rev. Mod. Phys. **61**, 689 (1989); M. C. Payne, M. P. Teter, D. C. Allan, T. A. Arias, and J. D. Joannopoulos, Rev. Mod. Phys. **64**, 1045 (1992).
- [7] K. Terakura, T. Oguchi, A. R. Williams, and J. Kübler, Phys. Rev. B **30**, 4734 (1984).
- [8] N. F. Mott and R. Peierls, Proc. Phys. Soc. (London) **A49**, 72 (1937).
- [9] N. F. Mott, Proc. Phys. Soc. (London) **A62**, 416 (1949).
- [10] J. Hubbard, Proc. Roy. Soc. (London) **A277**, 237 (1964).
- [11] V. I. Anisimov, J. Zaanen, and O. K. Andersen, Phys. Rev. B **44**, 943 (1991).
- [12] M. T. Czyżyk and G. A. Sawatzky, Phys. Rev. B **49**, 14211 (1994).
- [13] A. I. Liechtenstein, V. I. Anisimov, and J. Zaanen, Phys. Rev. B **52**, R5467 (1995).
- [14] T. Mizokawa and A. Fujimori, Phys. Rev. B **54**, 5368 (1996).
- [15] V. I. Anisimov, F. Aryasetiawan and A. I. Liechtenstein, J. Phys.: Cond. Mat. **9**, 767 (1997).
- [16] S. Y. Savrasov and G. Kotliar, Phys. Rev. Lett. **84**, 3670 (2000).
- [17] A. Georges, G. Kotliar, W. Krauth, and M. J. Rozenberg, Rev. Mod. Phys. **68**, 13 (1996).
- [18] S. Massida, M. Pasternak, A. Baldereschi, and R. Resta, Phys. Rev. Lett. **82**, 430 (1999).
- [19] S. Y. Savrasov and G. Kotliar, Phys. Rev. Lett. **90**, 056401 (2003).
- [20] U. D. Wdowik and K. Parlinski, Phys. Rev. B **75**, 104306 (2007).
- [21] L. Pintschovius, N. Pyka, W. Reichardt, A. Yu. Rumiantsev, N.L. Mitrofanov, A.S. Ivanov, G. Collin, and P. Bourges, Physica C **185**, 156 (1991).
- [22] R.J. McQueeney, Y. Petrov, T. Egami, M. Yethiraj, G. Shirane, and Y. Endoh, Phys. Rev. Lett. **82**, 628 (1999).
- [23] J.-H. Chung, T. Egami, R. J. McQueeney, M. Yethiraj, M. Arai, T. Yokoo, Y. Petrov, H. A. Mook, Y. Endoh, S. Tajima, C. Frost, and F. Dogan, Phys. Rev. B **67**, 014517 (2003).
- [24] N. Jinho Lee, K. Fujita, K. McElroy, J. A. Slezak, M. Wang, Y. Aiura, H. Bando, M. Ishikado, T. Matsui, J.-X. Zhu, A. V. Balatsky, H. Eisaki, S. Uchida, and J. C. Davis, Natura **442**, 546 (2006).

- [25] J. M. Tranquada, K. Nakajima, M. Braden, L. Pintschovius, and R. J. McQueeney, *Phys. Rev. Lett.* **88**, 075505 (2002).
- [26] M. Braden, W. Reichardt, S. Shiryayev, and S. N. Barilo, *Physica C* **378-381**, 89 (2002).
- [27] K. A. Chao, J. Spałek, A. M. Oleś, *J. Phys. C* **10**, L271 (1977).
- [28] T. Egami, S. Ishihara, and M. Tachiki, *Science* **261**, 1307 (1993); B. Bäuml, G. Wellein, and H. Fehske, *Phys. Rev. B* **58**, 3663 (1998).
- [29] A. S. Mishchenko and N. Nagaosa, *Phys. Rev. Lett.* **93**, 036402 (2004).
- [30] O. Rösch and O. Gunnarson, *Phys. Rev. Lett.* **93** 237001 (2004).
- [31] A. S. Alexandrov, J. Ranninger, and S. Robaszkiewicz, *Phys. Rev. Lett.* **56**, 949 (1986); R. Micnas, J. Ranninger, and S. Robaszkiewicz, *Rev. Mod. Phys.* **62**, 113 (1990); A. N. Das, J. Konior, D. K. Ray, and A. M. Oleś, *Phys. Rev. B* **44**, 7680 (1991).
- [32] Y. Tokura and N. Nagaosa, *Science* **288**, 462 (2000).
- [33] L. Martin-Carron and A. de Andres, *Eur. Phys. J. B* **22**, 11 (2001).
- [34] K.-Y. Choi, P. Lemmens, T. Sahaoui, G. Güntherodt, Yu. G. Pashkevich, V. P. Gnezdilov, P. Reutler, L. Pinsard-Gaudart, B. Büchner, and A. Revcolevschi, *Phys. Rev. B* **71**, 174402 (2005).
- [35] J. Bała, A. M. Oleś, and G. A. Sawatzky, *Phys. Rev. B* **65**, 184414 (2002).
- [36] D. Louca and T. Egami, *Phys. Rev. B* **59**, 6193 (1999); N. Mannella, A. Rosenhahn, C. H. Booth, S. Marchesini, B. S. Mun, S.-H. Yang, K. Ibrahim, Y. Tomioka, and C. S. Fadley, *Phys. Rev. Lett.* **92**, 166401 (2004).
- [37] I. V. Solovyev, *Phys. Rev. B* **69**, 134403 (2004); *J. Phys.: Cond. Mat.* **20**, 293201 (2008).
- [38] P. W. Anderson, *Phys. Rev.* **102**, 1008 (1956).
- [39] M. Nogues and P. Poix, *J. Phys. Chem. Solids* **23**, 711 (1962).
- [40] S.-H. Lee, C. Broholm, T. H. Kim, W. Ratcliff, S.-W. Cheong, *Phys. Rev. Lett.* **84**, 3718 (2000).
- [41] M. Schmidt, W. Radcliff, P. G. Radaelli, K. Refson, N. M. Harrison, S. W. Cheong, *Phys. Rev. Lett.* **92**, 056402 (2004).
- [42] A. B. Sushkov, O. Tchernyshyov, W. Ratcliff, S. W. Cheong, and H. D. Drew, *Phys. Rev. Lett.* **94**, 137202 (2005).
- [43] S. Bordacs, D. Varjas, I. Kezsmarki, G. Mihaly, L. Baldassarre, A. Abouelsayed, C. A. Kuntscher, K. Ohgushi, and Y. Tokura, *Phys. Rev. Lett.* **103**, 077205 (2009).
- [44] K. T. Moore and G. van der Laan, *Rev. Mod. Phys.* **81**, 235 (2009).
- [45] R. A. Reese, S. K. Sinha, and D. T. Peterson, *Phys. Rev. B* **8**, 1332 (1973).
- [46] J. Bouchet, F. Jollet, and G. Zerah, *Phys. Rev. B* **74**, 134304 (2006).

- [47] W. P. Crummett, H. G. Smith, R. M. Nicklow, and N. Wakabayashi, *Phys. Rev. B* **19**, 6028 (1979).
- [48] H. G. Smith, N. Wakabayashi, W. P. Crummett, R. M. Nicklow, G. H. Lander, and E. S. Fisher, *Phys. Rev. Lett.* **44**, 1612 (1980).
- [49] M. E. Manley, B. Fultz, R. J. McQueeney, C. M. Brown, W. L. Hults, J. L. Smith, D. J. Thoma, R. Osborn, and J. L. Robertson, *Phys. Rev. Lett.* **86**, 3076 (2001).
- [50] M. E. Manley, M. Yethiraj, H. Sinn, H. M. Voltz, A. Alatas, J. C. Lashley, W. L. Hults, G. H. Lander, and J. L. Smith, *Phys. Rev. Lett.* **96**, 125501 (2006).
- [51] J. Bouchet, *Phys. Rev. B* **77**, 024113 (2008).
- [52] X. Dai, S. Y. Savrasov, G. Kotliar, A. Migliori, H. Ledbetter, and E. Abrahams, *Science* **300**, 953 (2003).
- [53] J. Wong, M. Krisch, D. L. Farber, F. Occelli, A. J. Schwartz, T.-C. Chiang, M. Wall, C. Boro, and R. Xu, *Science* **301**, 1078 (2003).
- [54] G. R. Stewart, *Rev. Mod. Phys.* **56**, 755 (1984).
- [55] P. Strange, A. Svane, W. M. Tammerman, Z. Szotek, and H. Winter, *Nature* **399**, 756 (1999).
- [56] H. Olijnyk, W. A. Grosshans, and A. P. Jephcoat, *Phys. Rev. Lett.* **93**, 255505 (2004).
- [57] J. C. Glyden Houmann and R. M. Nicklow, *Phys. Rev. B* **1**, 3943 (1970).
- [58] R. M. Nicklow, N. Wakabayashi, and P. R. Vijayaraghavan, *Phys. Rev. B* **3**, 1229 (1971).
- [59] C. Stassis, T. Gould, O. D. McMaster, K. A. Gschneider, and R. M. Nicklow, *Phys. Rev. B* **19**, 5746 (1979).
- [60] G. Kresse and J. Furthmüller, *Comput. Mater. Sci.* **6**, 15 (1996).
- [61] P. E. Blöchl, *Phys. Rev. B* **50**, 17953 (1994).
- [62] G. Kresse and J. Joubert, *Phys. Rev. B* **59**, 1758 (1999).
- [63] J. P. Perdew, K. Burke, and M. Ernzerhof, *Phys. Rev. Lett.* **77**, 3865 (1996).
- [64] P. Söderlind, O. Eriksson, B. Johansson, and J. M. Wills, *Phys. Rev. B* **50**, 7291 (1994).
- [65] H. J. Monkhorst and J. D. Pack, *Phys. Rev. B* **13**, 5188 (1976).
- [66] J. Zaanen and G. A. Sawatzky, *J. Solid State Chem.* **88**, 8 (1990).
- [67] Z. Zhang and S. Satpathy, *Phys. Rev. B* **44**, 13319 (1991).
- [68] A. M. Oleś, G. Khaliullin, P. Horsch, and L. F. Feiner, *Phys. Rev. B* **72**, 214431 (2005).
- [69] D. van der Marel and G. A. Sawatzky, *Phys. Rev. B* **37**, 10674 (1988).
- [70] R. Feynman, *Phys. Rev.* **56**, 340 (1939).
- [71] K. Parlinski, Z. Q. Li, and Y. Kawazoe, *Phys. Rev. Lett.* **78**, 4063 (1997).

- [72] K. Parlinski, Software PHONON, Kraków, 2008.
- [73] P. Weiss and K. Renger, Arch. Elektrotechn. **11**, 279 (1914).
- [74] G. S. Parks and K. K. Kelly, J. Phys. Chem. **30**, 47 (1926); R. W. Millar, J. Am. Chem. Soc. **51**, 215 (1929).
- [75] E. J. W. Verwey, Nature (London) **144**, 327 (1939).
- [76] E. J. Verwey, P. W. Haayman, and F. C. Romeijan, J. Chem. Phys. **15**, 181 (1947).
- [77] E. J. Samuelsen, E. J. Bleeker, L. Dobrzynski, and T. Riste, J. Appl. Phys. **39**, 1114 (1968).
- [78] Y. Fujii, G. Shirane, and Y. Yamada, Phys. Rev. B **11**, 2036 (1975).
- [79] B. Lorenz and D. Ihle, Phys. Status Solidi B **96**, 659 (1979), D. Ihle and B. Lorenz, Phil. Mag. B **42**, 337 (1980).
- [80] S. M. Shapiro, M. Iizumi, and G. Shirane, Phys. Rev. B **14**, 200 (1976).
- [81] T. J. Moran and B. Lüthi, Phys. Rev. **187**, 710 (1969).
- [82] E. I. Terukov, W. Reichelt, D. Ihle, and H. Oppermann, Phys. Status Solidi B **95**, 491 (1979).
- [83] J. P. Sheperd, J. W. Koenitzer, R. Aragon, J. Spałek, and J. M. Honig, Phys. Rev. B **43**, 8461 (1991).
- [84] A. Kozłowski, Z. Kałol, D. Kim, R. Zalecki, J. M. Honig, Phys. Rev. B **54**, 12093 (1996).
- [85] P. Novak, H. Stepankova, J. English, J. Kohout, and V. A. M. Brabers, Phys. Rev. B **61**, 1256 (2000).
- [86] M. Mizoguchi, J. Phys. Soc. Jpn. **70**, 2333 (2001).
- [87] M. Iizumi, T. F. Koetzle, G. Shirane, S. Chikazumi, M. Matsui, and S. Todo, Acta Crystallogr., Sect. B: **B38**, 2121 (1982).
- [88] J. P. Wright, J. P. Attfield, and P. G. Radaelli, Phys. Rev. Lett. **87**, 266401 (2001); Phys. Rev. B **66**, 214422 (2002).
- [89] I. Leonov, A. N. Yaresko, V. N. Antonov, M. A. Korotin, and V. I. Anisimov, Phys. Rev. Lett. **93**, 146404 (2004).
- [90] H.-T. Jeng, G.Y. Guo, and D. J. Huang, Phys. Rev. Lett. **93**, 156403 (2004).
- [91] G. Subias, J. Garcia, J. Blasco, M. G. Proietti, H. Renevier, and M. C. Sanchez, Phys. Rev. Lett. **93**, 156408 (2004).
- [92] D. J. Huang, H.-J. Lin, J. Okamoto, K. S. Chao, H.-T. Jeng, G. Y. Guo, C.-H. Hsu, C.-M. Huang, D. C. Ling, W. B. Wu, C. S. Yang, and C. T. Chen, Phys. Rev. Lett. **96**, 096401 (2006).
- [93] E. Nazarenko, J. E. Lorenzo, Y. Joly, J. L. Hodeau, D. Mannix, and C. Martin, Phys. Rev. Lett. **97**, 056403 (2006).

- [94] J. Schlappa, C. Schübler-Langeheine, C. F. Chang, H. Ott, A. Tanaka, Z. Hu, M. W. Haverkort, E. Schierle, E. Weschke, G. Kaindl, and L. H. Tjeng, *Phys. Rev. Lett.* **100**, 026406 (2008).
- [95] Y. Joly, J. E. Lorenzo, E. Nazarenko, J.-L. Hodeau, D. Mannix, and C. Martin, *Phys. Rev. B* **78**, 134110 (2008).
- [96] J. E. Lorenzo, C. Mazzoli, N. Janouen, C. Detlefs, D. Mannix, S. Grenier, Y. Joly, and C. Marin, *Phys. Rev. Lett* **101**, 226401 (2008).
- [97] H. T. Stokes and D. M. Hatch, *COPL* software (2001).
- [98] H. T. Stokes and D. M. Hatch, *ISOTROPY* software (2002).
- [99] H. Shwenk, S. Bareiter, C. Hinkel, B. Lüthi, Z. Kąkol, A. Kozłowski, and J. M. Honig, *Eur. Phys. J. B* **13**, 491 (2000).
- [100] K. Siratori, Y. Ishii, Y. Morii, S. Funahashi, S. Todo, and A. Yanase, *J. Phys. Soc. Jpn.* **67**, 2818 (1998).
- [101] A. Yanase and K. Siratori, *J. Phys. Soc. Jap.* **53**, 312 (1984).
- [102] A. Yanase and N. Hamada, *J. Phys. Soc. Jpn.* **68**, 1607 (1999).
- [103] E. J. Samuelsen and O. Steinsvoll, *Phys. Status Solidi B* **61**, 615 (1974).
- [104] L. Degiorgi, I. Blatter-Mörke, and P. Wachter, *Phys. Rev. B* **35**, 5421 (1987).
- [105] L. V. Gasparov, D. B. Tanner, D. B. Romero, H. Berger, G. Margaritondo, and L. Forro, *Phys. Rev. B* **62**, 7939 (2000).
- [106] R. Gupta, A. K. Sood, P. Metcalf, and J. M. Honig, *Phys. Rev. B* **65**, 104430 (2002).
- [107] M. Sato, S. Kitao, Y. Kobayashi, R. Haruki, Y. Yoda, T. Mitsui, and T. Ishikawa, *Phys. Rev. Lett.* **91**, 185505 (2003).
- [108] B. Handke, A. Kozłowski, K. Parlinski, J. Przewoźnik, T. Ślęzak, A. I. Chumakov, L. Niesen, Z. Kąkol, and J. Korecki, *Phys. Rev. B* **71**, 144301 (2005).
- [109] S. K. Park, T. Ishikawa, and Y. Tokura, *Phys. Rev. B* **58**, 3717 (1998).
- [110] J. Garcia, G. Subias, J. Herrero-Martin, J. Blasco, V. Cuartero, M. C. Sanchez, C. Mazzoli, and F. Yakhou, *Phys. Rev. Lett.* **102**, 176405 (2009); S. B. Wilkins, S. Di Matteo, T. A. W. Beale, Y. Joly, C. Mazzoli, P. D. Hatton, P. Bencok, F. Yakhou, and V. A. M. Brabers, *Phys. Rev. B* **79**, 201102(R) (2009).
- [111] G. K. Rozenberg, M. P. Pasternak, W. M. Xu, Y. Amiel, M. Hanfland, M. Amboage, R. D. Taylor, and R. Jeanloz, *Phys. Rev. Lett.* **96**, 045705 (2006).
- [112] J. Spalek, A. Kozłowski, Z. Tarnawski, Z. Kąkol, Y. Fukami, F. Ono, R. Zach, L. J. Spalek, and J. M. Honig, *Phys. Rev. B* **78**, 100401(R) (2008).
- [113] A. Kozłowski, Z. Kąkol, and Z. Tarnawski, *Acta Phys. Pol. A* **111** 537 (2007).
- [114] J. L. Sarrao, L. A. Morales, J. D. Thomson, B. L. Scott, G. R. Stewart, F. Wastin, J. Rebizant, P. Boulet, E Colineau, and G. H. Lander, *Nature (London)* **420**, 297 (2002).

- [115] A. Szajek and J. A. Morkowski, *J. Phys.: Cond. Mat.* **15**, L155 (2003).
- [116] I. Opahle and P. M. Oppeneer, *Phys. Rev. Lett.* **90**, 157001 (2003).
- [117] T. Maehira, T. Hotta, K. Ueda, and A. Hasegawa, *Phys. Rev. Lett.* **90**, 207007 (2003).
- [118] J. J. Joyce, J. M. Wills, T. Durakiewicz, M. T. Butterfield, E. Guziewicz, J. L. Sarrao, L. A. Morales, A. J. Arko, and O. Eriksson, *Phys. Rev. Lett.* **91**, 176401 (2003).
- [119] P. Söderlind, *Phys. Rev. B* **70**, 094515 (2004).
- [120] A. B. Shick, V. Janiš, and P. M. Oppeneer, *Phys. Rev. Lett.* **95**, 016401 (2005).
- [121] L. V. Pourovskii, M. I. Katsnelson, and A. I. Lichtenstein, *Phys. Rev. B* **73**, 060506 (2006).
- [122] E. D. Bauer, J. D. Thompson, J. L. Sarrao, L. A. Morales, F. Wastin, J. Rebizant, J. C. Griveau, P. Javorsky, P. Boulet, E. Colineau, G. H. Lander, and G. R. Stewart, *Phys. Rev. Lett.* **93**, 147005 (2004).
- [123] Y. Bang, A. V. Balatsky, F. Wastin, and J. D. Thompson, *Phys. Rev. B* **70**, 104512 (2004).
- [124] N. J. Curro, T. Caldwell, E. D. Bauer, L. A. Morales, M. J. Graf, Y. Bang, A. V. Balatsky, J. D. Thompson, and J. L. Sarrao, *Nature (London)* **434**, 622 (2005).
- [125] P. B. Allen and R. C. Dynes, *Phys. Rev. B* **12**, 905 (1975).
- [126] W. L. McMillan, *Phys. Rev.* **167**, 331 (1968).
- [127] F. S. Khan and P. B. Allen, *Phys. Rev. B* **29**, 3341 (1984).
- [128] F. Jutier, G. A. Ummarino, J.-C. Griveau, F. Wastin, E. Colineau, J. Rebizant, N. Magnani, and R. Caciuffo, *Phys. Rev. B* **77**, 024521 (2008); G. A. Ummarino, N. Magnani, J.-C. Griveau, J. Rebizant, and R. Caciuffo, *J. Nucl. Phys.* **385**, 4 (2009).
- [129] S. Ikeda, Y. Tokiwa, T. Okubo, Y. Haga, E. Yamamoto, Y. Inada, R. Settai, and Y. Onuki, *J. Nucl. Sci. Technol.* **3**, 214 (2002).
- [130] I. Opahle, S. Elgazzar, K. Koepernik, and P. M. Oppeneer, *Phys. Rev. B* **70**, 104504 (2004).
- [131] R. Troć, Z. Bukowski, C. Sułkowski, H. Misiorek, J. A. Morkowski, A. Szajek, and G. Chełkowska, *Phys. Rev. B* **70**, 184443 (2004).
- [132] N. G. Nereson, C. E. Olsen, and G. P. Arnold, *Phys. Rev.* **135**, A176 (1964).
- [133] I. Turek, J. Kudrnovsky, M. Divis, P. Franek, G. Bihlmayer, and S. Blugel, *Phys. Rev. B* **68**, 224431 (2003).
- [134] J. Kunes and R. Laskowski, *Phys. Rev. B* **70**, 174415 (2004).
- [135] M. Seto, Y. Yoda, S. Kikuta, X. W. Zhang, and M. Ando, *Phys. Rev. Lett.* **74**, 3828 (1995).
- [136] A. I. Chumakov, R. Rüffer, O. Leupold, A. Barla, H. Thiess, J. M. Gil, H. V. Alberto, R. C. Vilao, and N. Ayres de Campos, V. G. Kohn, M. Gerken, and M. Lucht, *Phys. Rev. B* **63**, 172301 (2001).